Atmos. Chem. Phys., 15, 6159–6182, 2015
www.atmos-chem-phys.net/15/6159/2015/
doi:10.5194/acp-15-6159-2015

Atmospheric Chemistry and Physics
Open Access

Ozone and aerosol tropospheric concentrations variability analyzed using the ADRIMED measurements and the WRF and CHIMERE models

L. Menut[1], S. Mailler[1], G. Siour[2], B. Bessagnet[3], S. Turquety[1], G. Rea[1], R. Briant[1], M. Mallet[4], J. Sciare[5,6], P. Formenti[2], and F. Meleux[3]

[1]Laboratoire de Météorologie Dynamique, UMR CNRS8539, Ecole Polytechnique, Ecole Normale Supérieure, Université P.M.Curie, Ecole Nationale des Ponts et Chaussées, Palaiseau, France
[2]Laboratoire Inter-Universitaire des Systèmes Atmosphériques, UMR CNRS7583, Université Paris Est Créteil et Université Paris Diderot, Institut Pierre Simon Laplace, Créteil, France
[3]Institut National de l'Environnement Industriel et des Risques, Verneuil en Halatte, 60550, Parc Technologique ALATA, France
[4]Laboratoire d'Aérologie, UMR CNRS5560, Université P. Sabatier, Toulouse, France
[5]Laboratoire des Sciences du Climat et de l'Environnement (CNRS-CEA-UVSQ), Gif-sur-Yvette, France
[6]The Cyprus Institute, Energy Environment and Water Research Center, Nicosia, Cyprus

Correspondence to: L. Menut (menut@lmd.polytechnique.fr)

Received: 15 January 2015 – Published in Atmos. Chem. Phys. Discuss.: 2 February 2015
Revised: 14 April 2015 – Accepted: 13 May 2015 – Published: 5 June 2015

Abstract. During the months of June and July 2013, over the Euro–Mediterranean area, the ADRIMED (Aerosol Direct Radiative Impact on the regional climate in the MEDiterranean region) project was dedicated to characterize the ozone and aerosol concentrations in the troposphere. It is first shown that this period was not highly polluted compared to previous summers in this region, with a moderate ozone production, no significant vegetation fire events and several precipitation periods scavenging the aerosol. The period is modeled with the WRF (Weather Research and Forecasting) and CHIMERE models, and their ability to quantify the observed pollution transport events is presented. The CHIMERE model simulating all kinds of sources (anthropogenic, biogenic, mineral dust, vegetation fires); the aerosol speciation, not available with the measurements, is presented: during the whole period, the aerosol was mainly constituted by mineral dust, sea salt and sulfates close to the surface and mainly by mineral dust in the troposphere. Compared to the AERONET (Aerosol Robotic Network) size distribution, it is shown that the model underestimates the coarse mode near mineral dust sources and overestimates the fine mode in the Mediterranean area, highlighting the need to improve the model representation of the aerosol size distribution both during emissions, long-range transport and deposition.

1 Introduction

The Euro–Mediterranean region is surrounded by many urbanized and agricultural lands in the north and arid regions in the south. This leads to numerous different pollution sources with a majority of anthropogenic and biogenic sources in the north and mineral dust in the south. In addition, mainly during summer, vegetation fires are often observed. As previously studied by Moulin et al. (1998), Middleton and Goudie (2001), Kubilay et al. (2003) and Israelevich et al. (2012), among others, the summer period is characterized by a south to north flow from Africa, transporting mineral dust in the free troposphere, and a north to south flow transporting trace gases and particles of anthropogenic origin in the boundary layer, as summarized in Fig. 1.

In order to study the atmospheric composition over this region, the experimental part of the Aerosol Direct Radiative Impact on the regional climate in the MEDiterranean

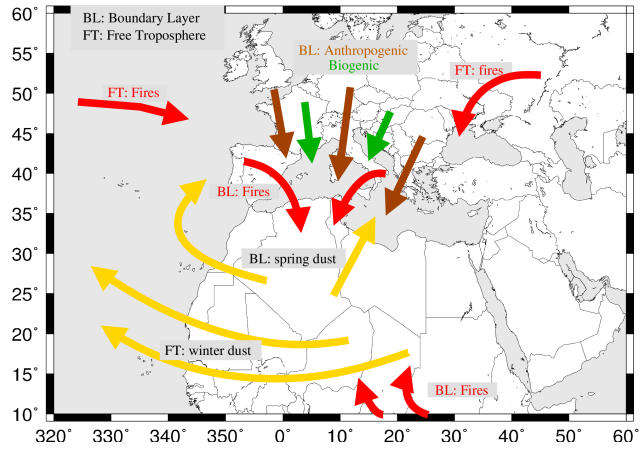

Figure 1. Synthesis of all aerosol types and transport pathways in the Mediterranean area. BL and FT stand for boundary layer and free troposphere, respectively.

region (ADRIMED) project (Mallet, 2014) was conducted during June and July 2013. ADRIMED is part of the international program ChArMEx (Chemistry–Aerosol Mediterranean Experiment; Dulac et al., 2013), aiming at assessing the present and future state of atmospheric chemistry in the Mediterranean area and its impact on regional climate, air quality, and marine ecosystems. This project completements several previous studies dedicated to the analysis of ozone and aerosols over the Mediterranean area.

Gerasopoulos et al. (2005) showed that ozone is controlled by production over the continent and may reach up to 60 ppb in the eastern Mediterranean marine boundary layer. Kalabokas et al. (2008) showed that the high concentrations observed are mainly driven by the anticyclonic meteorological conditions occurring during the summer. During the MINOS campaign (Mediterranean Intensive Oxidant Study; Lelieveld et al., 2002) over the same region, Roelofs et al. (2003) reported ozone concentrations in altitude of about 50 ppb, with peaks reaching 120 ppb. Lidar observations of ozone undertaken during the ESCOMPTE campaign (Expérience sur site pour contraindre les modèles de pollution atmosphérique et de transport d'émissions; Cros et al., 2004), in summer in the western part of the Mediterranean showed that highly concentrated plumes may be formed over a given country and transported for several hundreds of kilometers, before reaching ground levels (Colette et al., 2006).

Aerosols are also highly variable in space, time and composition. Their composition can be quantified by the relative contribution of various chemical species such as organic matter, sulfates, nitrates, ammonium, mineral dust and sea salt (Millan et al., 2005; Monks et al., 2009). Many experimental research programs were recently conducted to characterize the aerosol properties using surface measurements (Querol et al., 2009), airborne measurements (Dulac and Chazette, 2003), optical depths measured by sunphotometers (Kubilay et al., 2003), lidar measurements including EARLINET (European Aerosol Research LIdar Network to Establish an Aerosol Climatology; Papayannis et al., 2008; Pappalardo et al., 2014) or satellite data (Barnaba and Gobbi, 2004). Remotely sensed surface measurements are also used to better quantify the dust optical properties and direct radiative forcing as in Bergamo et al. (2008), Basart et al. (2009), Mallet et al. (2013), and di Sarra et al. (2008). The integrated project EUCAARI (dedicated to the Aerosol Climate Air Quality Interactions; Kulmala et al., 2011) was conducted to better characterize the aerosol life cycle and composition in Europe, integrating many types of aerosol studies, from the nano to the global scales, with a large scientific community.

These measurements have been accompanied by significant development in regional and global chemistry transport models (CTMs). For example, ozone was simulated using the CHIMERE regional CTM during the ESCOMPTE campaign (Menut et al., 2005) and the summertime ozone maximum was analyzed using the TOMCAT global CTM (Richards et al., 2013). Aerosol observations in the Mediterranean area often show large contributions from mineral dust, so that numerous studies were devoted to this species (Pérez et al., 2011; Nabat et al., 2012; Menut et al., 2013b; de la Paz et al., 2013). Their impact on climate via their radiative effect was recently analyzed with the models COSMO (Vogel et al., 2009), RegCM (Santese et al., 2010), SKYRON (Spyrou et al., 2013) and ALADIN-Climate (Nabat et al., 2014). Other important and still not well represented natural sources are now also included in CTMs. For example, sea salt was modeled in Jiménez-Guerrero et al. (2011) and vegetation fires in Turquety et al. (2014).

All these studies show that the ozone and aerosol are difficult to model in this region. Due to many different sources and their large variability, models have to include an accurate representation of all possible sources at the same time and of numerous chemical species. But, the more there is sources and chemistry, the more there are uncertainties in the modeling. To quantify the ability to retrieve the ozone and aerosol content and variability in the Euro–Mediterranean region, the WRF (Weather Research and Forecasting) and CHIMERE models are used to simulate the atmospheric composition from 1 June to 15 July 2013. A large domain, encompassing northern Africa and Europe, is designed to take into account all possible ozone precursors and aerosol sources and allows for contributions from long-range transport. The model results are compared to the available measurements and scores are presented. Having in mind the models' performances, the ozone and aerosol composition is further analyzed. For ozone, the variability is quantified both at the surface and in altitude. For aerosol, the model provides additional information such as composition and size distribution. Section 2 presents the experimental framework of the ADRIMED campaign and the whole set of data (surface, soundings, aircraft measurements, satellite) used in this study. Section 4 presents the modeling system and the settings. Section 5 ana-

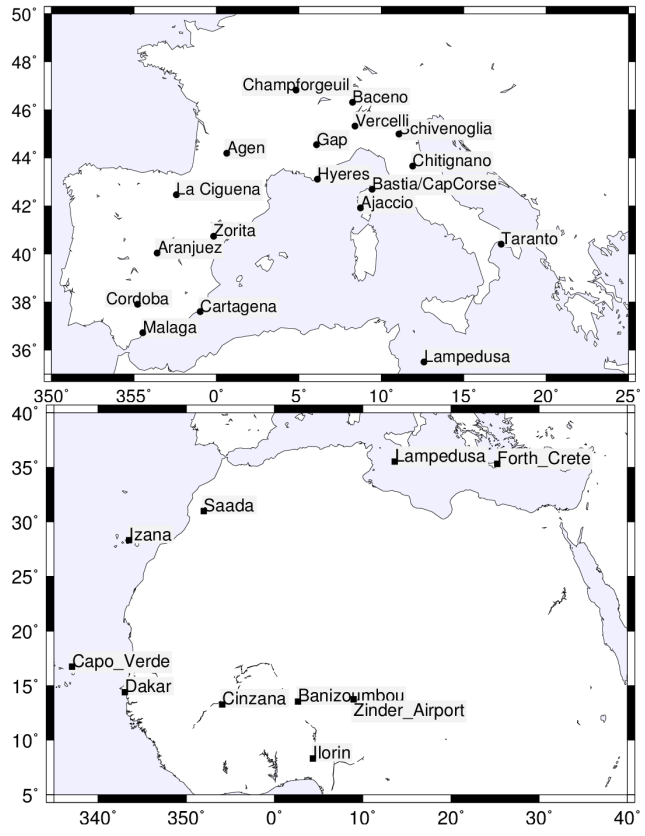

Figure 2. Locations of the AirBase (top) and AERONET (bottom) stations providing the O_3, PM_{10}, aerosol optical depth (AOD) and aerosol size distributions (ASD) measurements used in this study.

lyzes the meteorological situation using E-OBS data and the WRF model. Sections 6, 7 and 8 present ozone concentration, aerosol optical depth (AOD) and aerosol concentrations results, respectively. Sections 9 and 10 present aerosol speciation and size distribution. Conclusions and perspectives are presented in Sect. 11.

2 Observations

In order to characterize the meteorological situation and the atmospheric composition, and to estimate the realism of the models, many observations are used in this study. An overview of the pollution over the area is done with the MODIS (Moderate Resolution Imaging Spectroradiometer) satellite AOD measurements. With the surface measurements of the E-OBS database, the temperature and the precipitation are characterized. Using the EEA (European Environmental Agency) network, the surface ozone and particulate matter concentrations are studied. The optical depth is quantified using the AERONET (Aerosol Robotic Network) network. Temperature and ozone variabilities are estimated in the troposphere thanks to the aircraft observations of the ADRIMED project. The location of the measurement sites

Table 1. Characteristics of the ADRIMED, AirBase and AERONET stations used in this study. Note that the AirBase Italian stations of Chitignano, Baceno, Schivenoglia and Vercelli provide daily averaged values, when all other stations provide hourly (but not regular) measurements. The altitude is in meters above sea level (a.s.l.).

Site	Country	Longitude (°)	Latitude (°)	Altitude (m a.s.l.)
ADRIMED measurements sites				
Lampedusa	Italy	12.63	35.51	45.
Cape Corsica	France	9.41	42.83	533.
AirBase coastal "background" stations				
Zorita	Spain	−0.16	40.73	619.
Cartagena	Spain	−0.97	37.60	10.
Malaga	Spain	−4.46	36.72	36.
Ajaccio	France	8.73	41.92	28.
Bastia	France	9.44	42.69	57.
Hyères	France	6.13	43.11	33.
Taranto	Italy	17.28	40.41	10.
Chitignano	Italy	11.90	43.66	650.
AirBase continental "background" stations				
Aranjuez	Spain	−3.59	40.04	501.
Logroño	Spain	−2.42	42.46	386.
Cordoba	Spain	−4.77	37.90	119.
Agen	France	0.62	44.19	50.
Champforgeuil	France	4.83	46.82	46.
Gap	France	6.07	44.55	741.
Baceno	Italy	8.25	46.31	1637.
Schivenoglia	Italy	11.07	44.99	16.
Vercelli	Italy	8.40	45.31	131.
AERONET stations				
Banizoumbou	Nigeria	2.66	13.54	250.
Cabo Verde	Cabo Verde	−22.93	16.73	60.
Dakar	Senegal	−16.95	14.39	0.
Cinzana	Mali	−5.93	13.28	285.
Ilorin	Nigeria	4.340	8.32	350.
Izana	Spain	−16.49	28.31	2391.
Forth Crete	Greece	25.27	35.31	20.
Saada	Morocco	−8.15	31.61	420.
Zinder Airport	Nigeria	8.98	13.75	456.

used in this study is summarized in Table 1. Stations are sorted as a function of distance from the sea: the "coastal" stations are inland but less than 10 km from the coast and the "continental" stations are more than 10 km from the coast.

2.1 E-OBS meteorological measurements

Comparisons with the daily average 2 m temperature and precipitation amount taken from the European Climate Gridded data set (E-OBS; Haylock et al., 2008) are undertaken. This data set contains data collected from several thousands of meteorological stations throughout Europe and the Mediter-

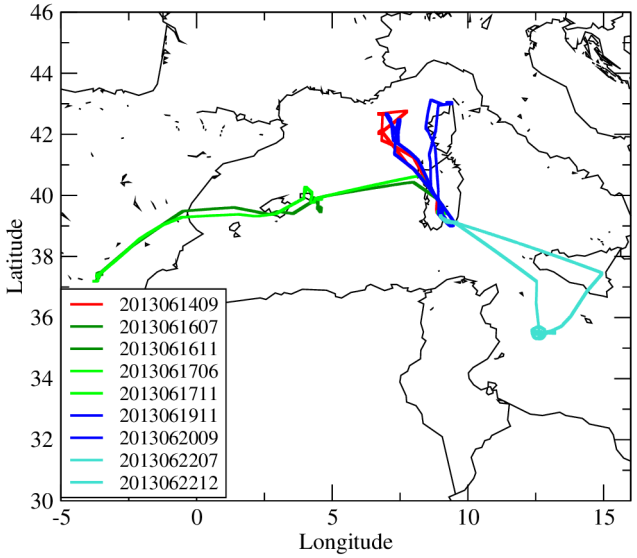

Figure 3. ATR-42 horizontal trajectories for the flights of 14 (red), 16 and 17 (blue), 19 and 20 (green) and 22 June (green-blue).

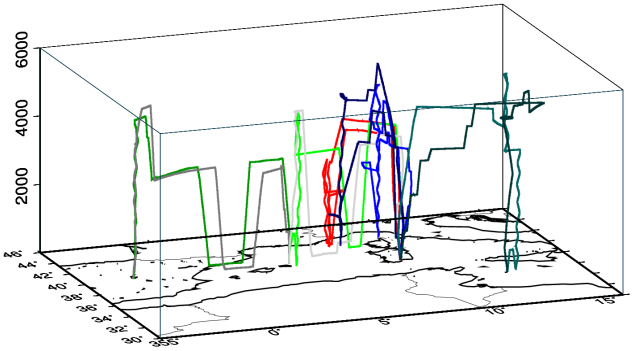

Figure 4. ATR-42 vertical trajectories for the flights of 14 (red), 16 and 17 (blue), 19 and 20 (green) and 22 June (green-blue).

Table 2. List of ATR flights for the tropospheric measurements of meteorological variables and ozone concentrations. N_{data} corresponds to the number of data after averaging the high temporal frequency of aircraft measurements to a constant 5 mn time step.

Flight no.	Date	J_{day}	Decimal hour	N_{data}
28	20130614	165	9.05	46
29	20130616	167	7.55	36
30	20130616	167	11.49	40
31	20130617	168	6.76	39
32	20130617	168	11.18	32
33	20130619	170	11.04	49
34	20130620	171	9.83	54
35	20130622	173	7.57	47
36	20130622	173	12.75	40

ranean area. These data are processed through a series of quality tests to remove errors and unrealistic values.

2.2 EEA chemical measurements

For regulatory pollutants, many measurements are routinely performed and well organized in quality-checked databases. The EEA (Guerreiro et al., 2013) is responsible for the AirBase database used in this study. It contains surface concentration measurements and information submitted by the participating countries throughout Europe (http://www.eea.europa.eu/). For this study, we focused on ozone and PM_{10}. In order to calculate scores and to study time series, a subset of data is used, including eight "coastal background" and nine "continental background" stations. Their location is displayed in Fig. 2 and details about their coordinates are provided in Fig. 1. They were chosen to be representative of various locations around the western Mediterranean Sea: Spain, France and Italy, including the Baleares, Corsica and Lampedusa islands. These stations are all "background" stations to ensure a correct representativity between the measured and the modeled values.

2.3 AERONET measurements

The AERONET photometer measurements (Holben et al., 2001) are used to characterize the observed AOD and the volume aerosol size distribution (ASD). The AOD data are recorded by numerous stations deployed around the world and hourly values are available. Several quality levels are proposed on the AERONET database (http://aeronet.gsfc.nasa.gov/). In this study, the level 2.0 is used for AOD and the level 1.5 for ASD (Dubovik and King, 2000). The stations used in this study are listed in Table 1 and their location is displayed in Fig. 2.

2.4 ADRIMED measurements

The experimental part of the ADRIMED experiments includes surface measurements (at the supersites of Cape Corsica and Lampedusa), remote sensing and airborne measurements, as presented in Mallet (2014). The airborne measurements are analyzed for ozone concentrations. These measurements were performed onboard the ATR-42 aircraft (operated by the SAFIRE CNRS, CNES and Météo-France joint laboratory). Nine flights were conducted during the studied period. The flight numbers, date and decimal hour, and corresponding day of flight are reported in Table 2. Trajectories are very different from one flight to another and are represented in Fig. 3 on a map and in Table 4 to see the vertical extension of the flights.

3 Air quality during the ADRIMED period

The first step is to evaluate if the ADRIMED period was highly polluted or not, compared to previous summers in this

Table 3. Number of days in June, July and August when (i) surface daily mean concentrations of PM_{10} exceed the threshold value of 30 µg m^{-3}, and (ii) surface daily maximum concentrations of ozone exceeds 120 µg m^{-3}. Data are extracted from the model cell corresponding to the location.

Occurrence of PM_{10} daily mean > 30 µg m^{-3}					
Year	Madrid	Barcelona	Marseille	Rome	Athens
2007	17	7	6	8	8
2008	12	6	7	8	2
2009	13	13	10	2	2
2010	20	39	18	24	57
2011	1	4	11	2	15
2012	12	10	28	0	8
2013	7	14	28	3	6
Occurrence of ozone daily max > 120 µg m^{-3}					
Year	Madrid	Barcelona	Marseille	Rome	Athens
2007	6	5	17	8	42
2008	21	18	29	44	66
2009	18	29	34	31	40
2010	21	18	35	28	62
2011	19	2	12	18	37
2012	12	8	15	31	45
2013	32	12	31	33	15

region. To quantify this air quality, we used the results of the MACC-II (Monitoring Atmospheric Composition and Climate) and MACC-III projects for the surface O_3 and PM_{10}.

The surface concentrations are calculated from a multi-ensemble of reanalysis based on seven European models (CHIMERE, EMEP, EURAD-IM, LOTOS-EUROS, MATCH, MOCAGE and SILAM) and mostly relying upon validated in situ observation data sets for the period between 2007 and 2012 and near-real time observations for 2013. Details of the models in their operational setup are presented in Marécal et al. (2015). This production has been established by the GEMS FP6 project and its follow-up FP7 projects (MACC, MACC-II and MACC-III). The IFS meteorological fields from ECMWF, the TNO-MACC emission inventory, (Kuenen et al., 2014), and the global chemical boundary conditions from MACC reanalysis or forecasts according to availability are used to force the models. Then, each model uses its own assimilation system (from optimal interpolation to 4D-VAR) to compute the analyses which allow building the ensemble. The ensemble hourly values are produced throughout Europe from the median value of the Ensemble and at $0.1° \times 0.1°$ resolution.

To estimate the relative air quality of the summer 2013, compared to previous summers, two indicators are computed. These indicators are both estimated for locations corresponding to highly urbanized cities, around the Mediterranean Basin. A subset of data is selected to focus on the months of June, July and August of each year. First, the daily mean surface concentrations of PM_{10} are calculated. The days when these values exceed 30 µg m^3 are counted. Second, the daily maximum of surface ozone concentrations is calculated. The days when these values exceed 120 µg m^3 are counted. The results are presented in Table 3. For surface PM_{10}, the less polluted summer is 2011; 2013 also exhibits low values (except in Marseille). All other years present their highest occurrences of PM_{10} higher than 30 µg m^{-3}. For surface ozone, 2011 remains the less polluted summer for these cities. 2013 is in the range of the other years, but remains lower than the summers of 2008, 2009 and 2010. Finally, summer 2013 can be considered as moderately polluted, compared to the years between 2007 and 2013.

4 Modeling system

The modeling system is composed of several models: the WRF regional meteorological model, the CHIMERE CTM and additional individual models dedicated to emission flux estimations. All these models are integrated in a modeling platform usable both in analysis and forecast modes. The simulation was performed from 1 June to 15 July 2013.

4.1 WRF meteorological model

The meteorological variables are modeled with the non-hydrostatic WRF regional model in its version 3.5.1 (Skamarock et al., 2007). The global meteorological analyses from NCEP/GFS (Kalnay et al., 1996) are provided on a regular $1.125° \times 1.125°$ grid. They are hourly read by WRF using nudging techniques for the main atmospheric variables (pressure, temperature, humidity, wind). In order to preserve both large-scale circulations and small-scale gradients and variability, the "spectral nudging" was chosen. This nudging was evaluated in regional models, as presented in Von Storch et al. (2000). In this study, the spectral nudging was selected to be applied for all wavelengths greater than ≈ 2000 km (wave numbers less than 3 in latitude and longitude, for wind, temperature and humidity and only above 850 hPa). This configuration allows the regional model to create its own structures within the boundary layer but makes sure it follows the large-scale meteorological fields.

In this study, the model is used with a constant horizontal resolution of 60 km × 60 km and 28 vertical levels from the surface to 50 hPa, as displayed in Fig. 5. The Single Moment-5 class microphysics scheme is used, allowing for mixed-phase processes and supercooled water (Hong et al., 2004). The radiation scheme is the RRTMG scheme with the MCICA method of random cloud overlap (Mlawer et al., 1997). The surface layer scheme is based on Monin–Obukhov with the Carslon–Boland viscous sublayer scheme. The surface physics is calculated using the Noah Land Surface Model scheme with four soil temperature and mois-

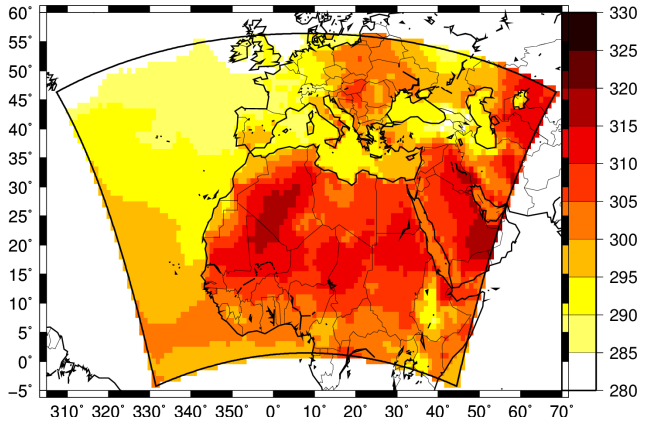

Figure 5. The simulation domain for WRF and CHIMERE. A Lambert conformal projection is used with a constant horizontal resolution of 60 km × 60 km. Colors represent the 2 m temperature (in Kelvin) for 21 June 12:00 UTC.

ture layers (Chen and Dudhia, 2001). The planetary boundary layer physics is processed using the Yonsei University scheme (Hong et al., 2006) and the cumulus parameterization uses the ensemble scheme of Grell and Devenyi (2002).

4.2 CHIMERE chemistry-transport model

CHIMERE is a CTM allowing the simulation of concentration fields of gaseous and aerosol species at a regional scale. It is an offline model, driven by precalculated WRF meteorological fields. In this study, the version fully described in Menut et al. (2013a) is used. The simulations are performed over the same horizontal domain as the one defined for WRF, with a constant resolution of 60 km × 60 km. The 28 vertical levels of the WRF simulations are projected onto 20 levels from the surface up to 300 hPa.

The chemical evolution of gaseous species is calculated using the MELCHIOR2 scheme and that of aerosols using the scheme developed by Bessagnet et al. (2004). This module takes into account sulfate, nitrate, ammonium, primary organic matter (POM), elemental carbon (EC), secondary organic aerosols (SOA), sea salt, dust and water. The aerosol size is represented using 10 bins, from 40 nm to 40 µm in diameter. The aerosol life cycle is completely represented with nucleation of sulfuric acid, coagulation, adsorption/desorption, wet and dry deposition and scavenging. This scavenging is represented by both coagulation with cloud droplets and precipitation. The formation of SOA is also taken into account.

The photolysis rates are explicitly calculated using the FastJX radiation module (version 7.0b; Wild et al., 2000; Bian et al., 2002). The modeled AOD is calculated by FastJX and for several wavelengths: 200, 300, 400, 600 and 1000 nm. For the comparisons with the AERONET measurements, we selected the AOD calculated at 600 nm. This calculation includes absorption by ozone (over the whole atmospheric column), Rayleigh scattering, Mie diffusion by liquid water and ice water clouds, absorption and Mie diffusion by aerosols. In this model version, the aerosol is dry. A complete analysis of the improvement obtained in the model with this online calculation is fully described in a companion paper (Mailler et al., 2015).

At the boundaries of the domain, climatologies from global model simulations are used. In this study, outputs from LMDz-INCA (Szopa et al., 2009) are used for all gaseous and aerosol species, except for mineral dust. For this species, simulations from the GOCART model are used (Ginoux et al., 2001).

The anthropogenic emissions are estimated using the same methodology as the one described in (Menut et al., 2012) but with the HTAP (hemispheric transport of air pollution) annual totals as input data. These masses were prepared by the EDGAR team, using inventories based on MICS-Asia, EPA-US/Canada and TNO databases (http://edgar.jrc.ec.europa.eu/national_reported_data/htap.php). Biogenic emissions are calculated using the MEGAN emissions scheme (Guenther et al., 2006) which provides fluxes of isoprene and monoterpenes. In addition to this version, several processes were improved and added in the framework of this study. First, the mineral dust emissions are now calculated using new soil and surface databases, (Menut et al., 2013b) and with a spatial extension of potentially emitting areas in Europe as described in Briant et al. (2014).

Emission fluxes produced by biomass burning are estimated using the new high-resolution fire model presented in Turquety et al. (2014). Taking into account these fluxes is a major improvement in the CHIMERE model. Figure 6 presents the locations of burned areas during the summer of 2013, as detected by the MODIS satellite-based instrument (MCD64 product at 500m resolution, processed as described in Turquety et al. (2014), and gridded onto the CHIMERE grid). The week number of first fire detection within each model grid cell ranges from 1 (the first week of June 2013) to 12 (the last week of September 2013). It shows that a majority of the first fire events occurred during weeks 8–12, i.e., during September. These fires are mainly located in Portugal and Russia and, to a lesser extent, Greece. For each model grid cell, the number of fire events is presented (i.e., the number of area-burned detections). For a large majority of diagnosed fires, this number is 1, showing there were not a lot of fires during the summer of 2013.

5 Modeled meteorology evaluation

The meteorological modeling was already done and evaluate with the WRF model, for the same kind of domain and resolution as in Mailler et al. (2013) and Menut et al. (2013b, c) for example. It was shown that the model is able to accurately reproduce the main meteorological variables over the Euro–

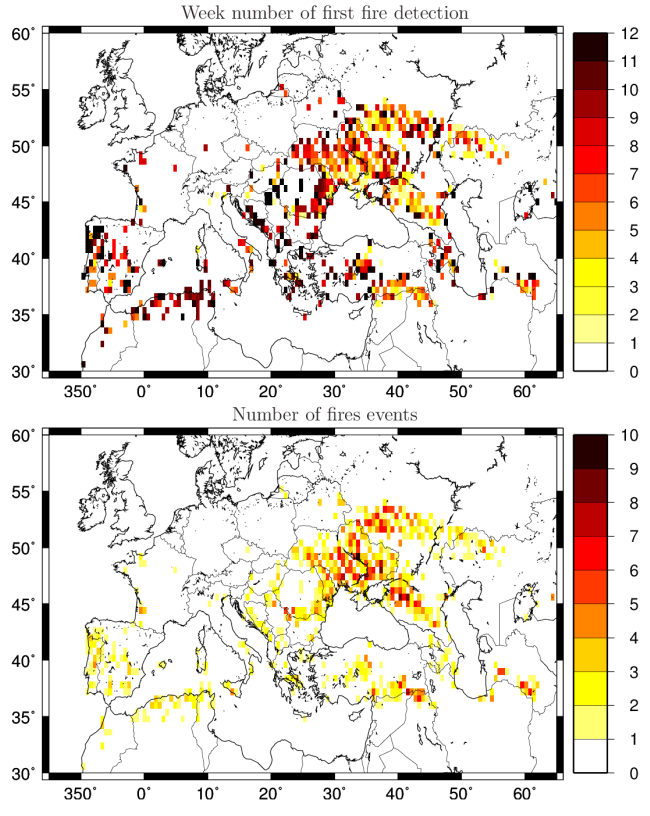

Figure 6. Synthesis of vegetation fires events observed during the summer of 2013, from the 1 June to the 31 August. [top] week of first detection, [bottom] number of events.

Mediterranean area: the day-to-day and hourly variabilities are well reproduced for all variables, the biases are known and the model representativity is adapted to the main variations of gaseous and aerosol formation and transport. However, since the model performance is variable for different regions, the 2 m temperature and the precipitation amount are here compared to the available data of E-OBS.

5.1 Daily maps

A comparison of 2 m temperature, T_{2m}, (K) and precipitation amount, Pr, (mm day^{-1}) is presented in Fig. 7. Three days are selected, 16, 20 and 24 June 2013, corresponding to examples every 4 days during the ADRIMED experiment. For each day and for the WRF results, the hourly 2 m temperature is averaged over the day and the hourly precipitation amount (mm h^{-1}) is cumulated to have millimeters per day. For the E-OBS observations, values are available over land only. For the WRF model, 2 m temperature and precipitation amount are available over the whole model domain, even if this domain is limited to a maximum latitude of 55° N.

For the 2 m temperature, we note that the observed and modeled values are close. For example, over Germany, a maximum of T_{2m} is observed during 20 June, also well modeled by WRF. For Pr, the main structures and the relative amount are also well modeled. For 16 June, the E-OBS data diagnosed precipitations in the western part of United Kingdom, France and Spain. WRF is able to modeled this pattern and shows a large precipitation system over the Atlantic Ocean. This system is advected to the eastern part of Europe and the WRF model is able to reproduce this advection speed as well as the accumulated precipitation values. These comparisons show the model is able to reproduce the main synoptic-scale absolute values and variability observed during this period.

5.2 Daily time series

From the E-OBS data daily maps, time series are extracted for some sites in Europe, as listed in Fig. 1. From 1 June to 15 July, for the grid cell corresponding to the site location, daily averages of the WRF model hourly results are computed for the 2 m temperature, and values are cumulated for precipitation. These comparisons are displayed in Fig. 8 and statistical scores are presented in Table 4.

For T_{2m}, the scores show that the correlation is high, ranging from 0.87 to 0.99. However, a non-negligible bias is calculated, ranging between −4.1 and 0.87 K, showing the model mainly underestimates the E-OBS gridded values. This bias cannot be attributed to a problem of measurements versus model representativity, the E-OBS values being regridded with a 0.25° × 0.25° resolution and the model having a 60 km × 60 km horizontal resolution. This bias is more probably due to the boundary layer or microphysics schemes used with WRF in this study. The model is able to reproduce the main variability observed during the whole period: low temperatures observed in the first days of June, corresponding to precipitation events, then a warm period, with temperature increasing from ≈ 290 to ≈ 295 K in the period of 14–17 June. A second large precipitation event is observed from 18 to 25 June (except in Bastia) leading to a slight cooling. After 25 June, precipitations are observed and modeled but they are more moderate and the temperature increases from ≈ 290 to ≈ 295 K until the end of the studied period, 14 July 2013.

The daily precipitation amount Pr has to be analyzed differently than the temperature. For the temperature, the model has to provide a correct space and time variability and a bias as low as possible. For the precipitation, the space and time variability is the most important since for chemistry-transport modeling, when a precipitation event is diagnosed, the atmospheric column is scavenged. This is why, in place of correlation, we introduce here the hit rate score: for a threshold arbitrarily chosen as $Pr_T = 0.1$ mm day^{-1} (i.e., there is precipitation for this day and this site), the event is considered as true if $Pr > Pr_T$. If this condition is reached for the observations and the model, a counter increments the a value. If the condition is reached for the observations and not the

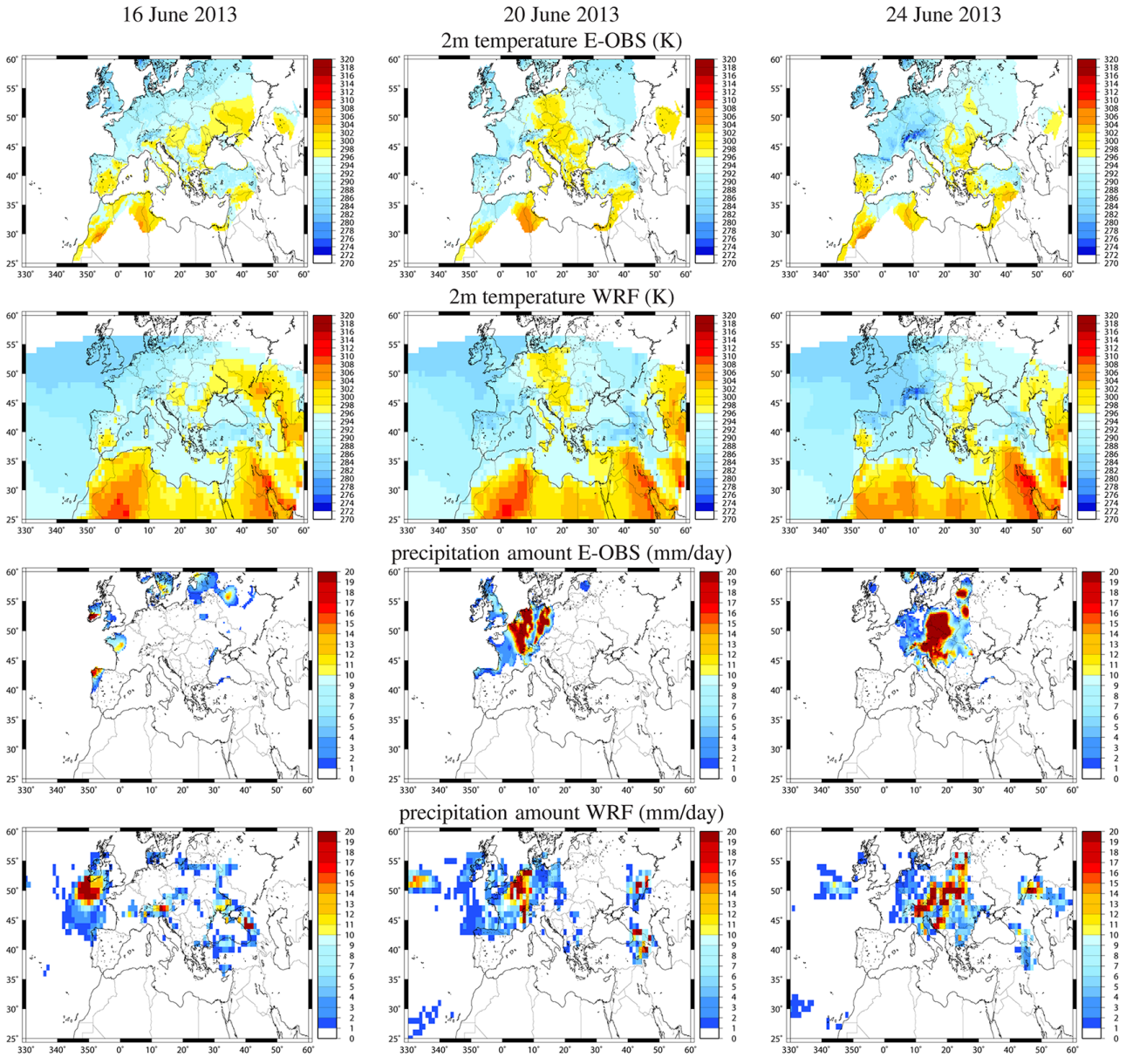

Figure 7. Comparison of daily mean averaged 2 m temperature (K) and daily accumulated precipitation amount (mm day^{-1}) with E-OBS (available over land only) and the WRF meteorological model.

model, a counter increments the c value. The hit rate, HR, is defined as

$$\mathrm{HR} = \frac{a}{a+c}. \quad (1)$$

The target value for the hit rate is 1, meaning that the model was able to catch all the observed events. Results are presented in Table 5. The number of events is also displayed since precipitations did not occur every day. The number of days under a precipitation event is between 1 and 19 for a total of 41 studied days. The HR ranges from 0.64 to 1, showing that the model reproduces this variable fairly well. One also notes that the mean bias is often negative, showing that the modeled precipitations are lower than what was observed.

6 Analysis of ozone concentrations

The first comparisons between measured and modeled atmospheric composition are undertaken for the analysis of ozone concentrations near the surface and in altitude. Ozone reflects the amount of photo-oxidant pollution, especially during summertime periods. Two kinds of data are used in this section: (i) the routine surface measurements of the AirBase

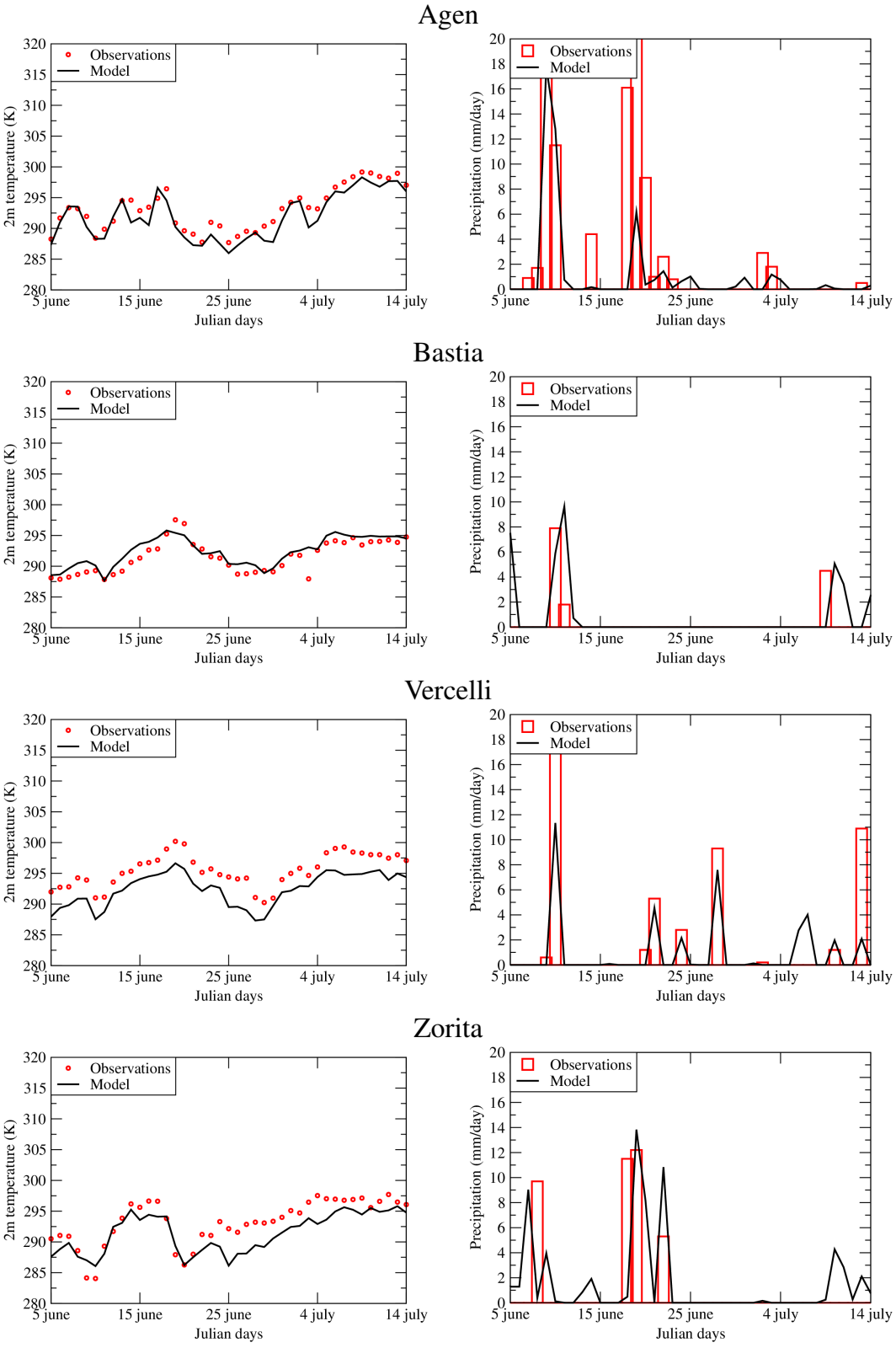

Figure 8. Time series of daily mean averaged 2 m temperature (K) and daily precipitation amount (mm day^{-1}) for several sites where chemical measurements are also available. Time series are extracted from maps of E-OBS daily data.

Table 4. Correlations (R), root mean squared error (RMSE) and bias of measured and modeled daily mean averaged values of 2 m temperature (K). The bias expressed the (model) minus (observations) values.

Site	T_{2m} daily mean (K)		R	RMSE	Bias
	Obs.	Mod.			
Cape Corsica	293.18	292.26	0.89	1.54	−0.92
Zorita	293.22	291.41	0.87	2.54	−1.81
Bastia	291.55	292.42	0.90	1.46	0.87
Chitignano	293.61	291.63	0.94	2.19	−1.98
Aranjuez	297.33	295.63	0.99	1.83	−1.70
Logroño	290.00	287.88	0.96	2.42	−2.11
Cordoba	298.15	296.20	0.98	2.06	−1.96
Agen	293.11	291.90	0.95	1.64	−1.20
Champforgeuil	292.64	289.25	0.96	3.50	−3.39
Gap	289.61	287.59	0.96	2.21	−2.02
Baceno	287.89	283.80	0.95	4.21	−4.10
Schivenoglia	296.28	294.17	0.96	2.26	−2.12
Vercelli	295.51	292.46	0.95	3.17	−3.05

Table 5. Hit rate (HR) and bias of measured and modeled daily mean averaged values of precipitation amount (mm day^{-1}). The bias expressed the (model) minus (observations) values.

Site	N_{obs}	Pr (mm day^{-1})		HR	Bias
		Obs.	Mod.		
Cape Corsica	3	2.10	0.97	0.67	−1.13
Zorita	4	9.68	6.38	1.00	−3.29
Bastia	3	4.73	5.18	0.67	0.45
Chitignano	6	4.12	3.79	0.83	−0.33
Aranjuez	1	1.20	0.93	1.00	−0.27
Logroño	11	6.73	5.73	1.00	−1.00
Cordoba	1	1.40	0.11	1.00	−1.29
Agen	14	7.16	2.91	0.64	−4.25
Champforgeuil	13	7.12	4.11	0.92	−3.01
Gap	8	6.53	9.41	0.75	2.89
Baceno	19	4.73	11.95	1.00	7.22
Schivenoglia	6	6.87	2.44	0.83	−4.42
Vercelli	9	5.59	3.30	0.67	−2.29

background stations and (ii) the airborne measurements done for ADRIMED with the ATR aircraft. The AirBase measurements are regular in time (hourly), and are used to quantify if the model is able to simulate both the background values and the peaks during high-pollution events. However, being only at the surface, these measurements are not dedicated to provide information on the model behavior in the whole troposphere. Thus, they do not allow for an interpretation on the ozone long-range transport. The ATR measurements are then complementary, providing vertical ozone profiles at a given time. However, unlike surface observations, they are very specific and do not reflect the overall situation of atmospheric pollution over the whole Mediterranean area.

6.1 Ozone surface concentration maps

Simulated surface ozone concentrations are displayed in Fig. 9. The three maps are selected to present values for the same days as for the meteorological variables in Fig. 7. For 16 June 2013, over the Mediterranean Sea, ozone values vary a lot, between 30 and 70 µg m^{-3}, with several plumes having a spatial extent of a few tens of kilometers only. The highest surface concentrations are modeled in the southeastern part of the domain, over Saudi Arabia. Surface concentrations are much higher on 20 June 2013 over Europe. This corresponds to the highest T_{2m} values, enhancing the photochemical processes over anthropogenic sources such as Belgium and the Netherlands. Over Great Britain and France, values are low and this corresponds to cloudiness associated with the observed and modeled precipitations. On 24 June, ozone concentrations are low (less than 40 µg m^{-3}) over all of Europe. This corresponds to the advection of this precipitation event from west to east. Finally, these maps show that ozone concentrations were moderate during this ADRIMED period, except over Saudi Arabia.

6.2 Ozone surface concentrations time series

To better understand the daily variability observed on the maps, scores are calculated for daily maximum and daily mean averaged values. Results are presented in Table 6 (daily maximum) and Table 7 (hourly values). The corresponding time series are presented in Fig. 10 for the daily maximum values.

The scores reported in Table 6 show the ability of the model to capture extreme events. Depending on the location, the model simulates lower or higher maximum daily values compared to the measurements. But for all stations, the differences between the two is never more than 20 µg m^{-3}. The correlations are also very dispersed, with values ranging from 0.15 (Malaga) to 0.71 (Agen). One can expect to have better correlations over the continent than over the sea due to the formation processes of ozone. This is not always the case, showing the difficulty of the model to estimate daily peaks over this complex region.

The scores in Table 7 are complementary and present results for hourly values. In this case, the complete diurnal cycle of ozone formation is taken into account. The scores are often better than for the daily peaks, with values of up to 0.81 (Cordoba). The low-correlation results are obtained for Ajaccio and Malaga (0.40), Bastia (0.29) and Gap (0.36), as already diagnosed with the daily peaks. This denotes a general inability of the model to represent ozone formation and transport over these areas. For these three sites, the problem is probably related to the low model resolution, these three

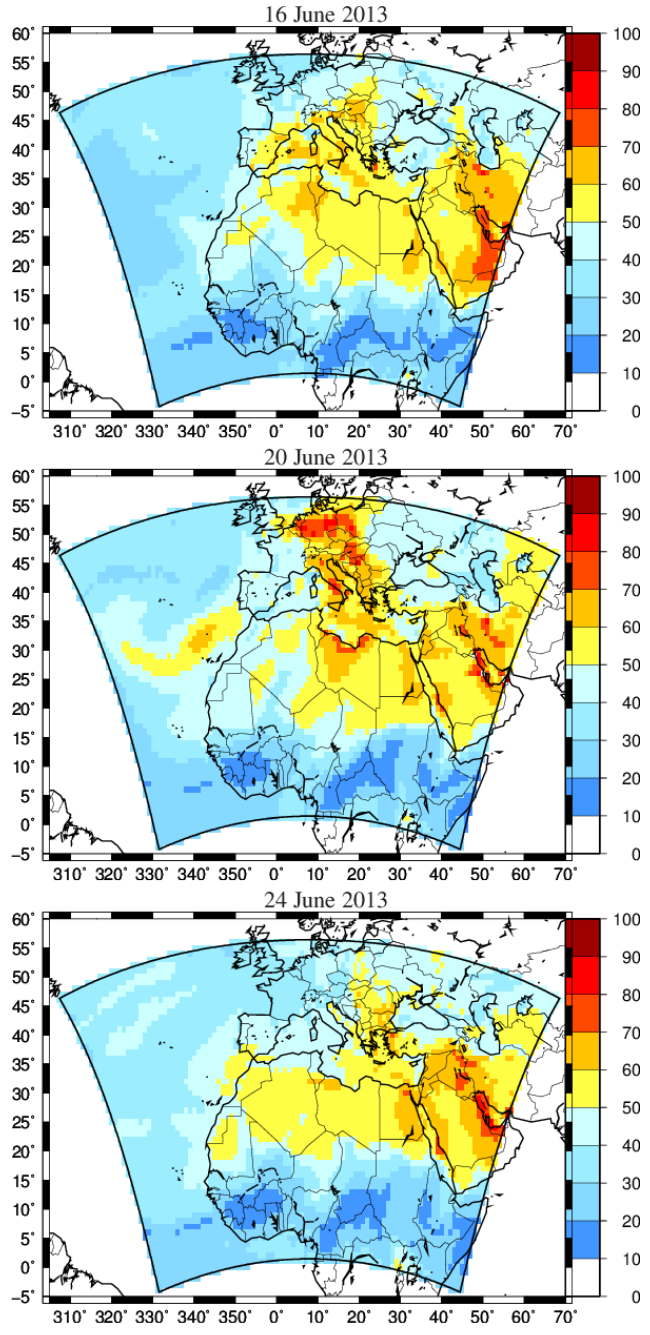

Figure 9. Modeled surface ozone concentrations (µg m^{-3}) for 16, 20 and 24 June 2013 at 12:00 UTC.

sites being in mountainous or insular areas, the subgrid-scale variability of ozone remains difficult to model.

Time series of measured and modeled ozone daily maximum are displayed in Fig. 10. For the coastal stations, Ajaccio, Bastia and Zorita, the measured values show flatter time series than the modeled ones, explaining low correlations obtained in Ajaccio and Bastia. When the model overestimates the concentrations in Ajaccio, it underestimates the concentrations in Bastia, even if the locations are close and located

Table 6. R, RMSE and bias of measured and modeled daily maximum value of surface O_3 concentrations (µg m^{-3}), for AirBase stations.

Site	N_{obs}	O_3 daily max		R	RMSE	Bias
		Obs.	Mod.			
AirBase coastal "background" stations						
Zorita	37	110.6	105.0	0.66	14.8	−5.6
Cartagena	41	102.4	113.1	0.47	16.2	10.7
Malaga	40	113.6	101.0	0.15	24.2	−12.6
Ajaccio	38	107.2	100.9	0.39	18.0	−6.3
Bastia	41	114.8	97.3	0.21	25.0	−17.5
Hyères	41	118.6	95.7	0.55	29.3	−22.9
Taranto	41	116.8	123.3	0.70	12.8	6.5
Chitignano	40	99.4	110.2	0.56	20.5	10.8
AirBase continental "background" stations						
Aranjuez	38	113.3	112.2	0.38	22.0	−1.0
Logroño	41	102.3	97.5	0.55	21.6	−4.9
Cordoba	41	127.3	113.1	0.60	21.0	−14.2
Agen	41	95.3	95.8	0.71	19.3	0.5
Champforgeuil	38	99.3	99.5	0.54	21.3	0.3
Gap	39	98.4	103.9	0.32	16.8	5.6
Baceno	39	117.0	104.6	0.29	21.5	−12.4
Vercelli	39	124.4	129.2	0.61	26.0	4.8

Table 7. R, RMSE and bias of measured and modeled of hourly surface O_3 concentrations (µg m^{-3}), for AirBase stations.

Site	N_{obs}	O_3 hourly		R	RMSE	Bias
		Obs.	Mod.			
AirBase coastal "background" stations						
Zorita	815	74.0	84.7	0.71	28.2	10.7
Cartagena	956	73.4	93.9	0.59	29.7	20.5
Malaga	907	87.2	87.4	0.40	23.5	0.2
Ajaccio	892	73.0	79.8	0.40	26.1	6.8
Bastia	978	90.8	76.4	0.29	27.8	−14.4
Hyères	983	86.5	68.2	0.64	29.1	−18.3
Taranto	575	90.1	98.5	0.74	19.0	8.4
Chitignano	892	72.4	89.4	0.55	27.6	17.0
AirBase continental "background" stations						
Aranjuez	841	79.7	82.9	0.67	21.3	3.2
Logroño	978	72.3	79.1	0.66	22.9	6.8
Cordoba	945	91.0	89.4	0.81	17.2	−1.6
Agen	977	64.6	74.9	0.73	23.0	10.3
Champforgeuil	836	61.9	76.2	0.67	31.1	14.3
Gap	917	66.1	91.4	0.36	35.5	25.3
Baceno	913	86.3	91.3	0.62	19.6	5.1
Vercelli	898	85.1	93.1	0.68	26.8	8.0

in the island of Corsica. From a model point of view, this consists in two close (but not neighboring) grid cells. These high differences may be explained by zooming in on Corsica, as displayed in Fig. 11: ozone surface concentrations (in ppb)

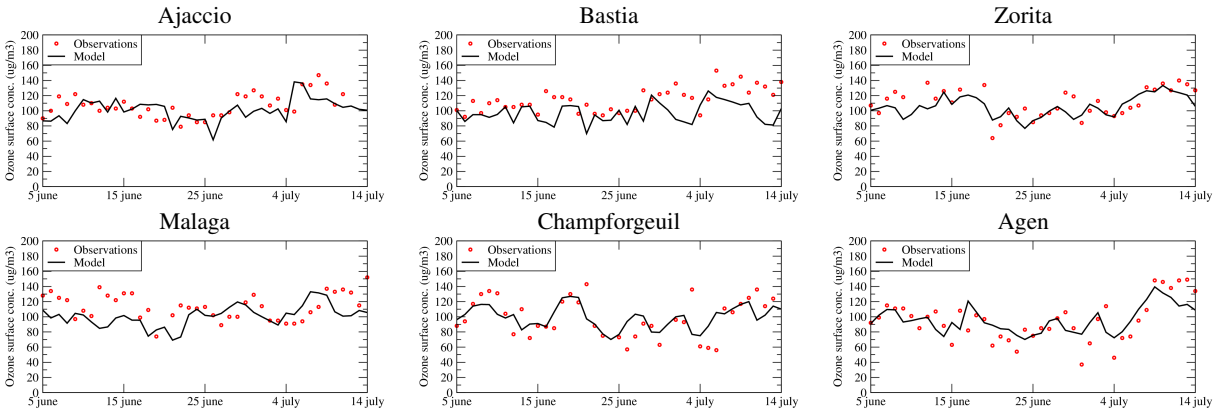

Figure 10. Time series of daily maximum of O_3 surface concentrations for some selected AirBase sites, continental and coastal stations.

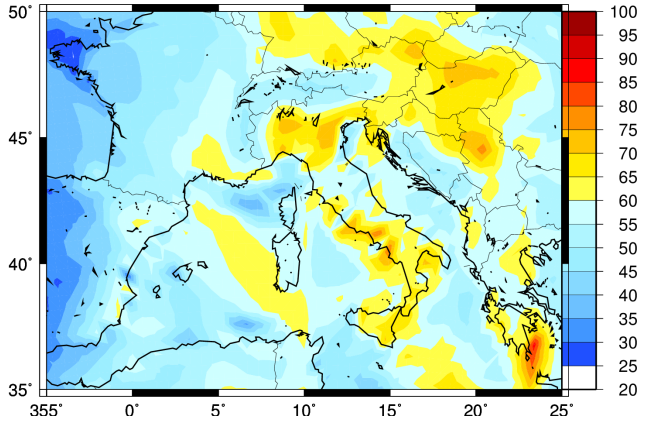

Figure 11. Surface ozone concentrations (ppb) map for 17 June 2013, 12:00 UTC.

are shown for 17 June 2013, 12:00 UTC, as an example. For this day, and more generally for the whole ADRIMED period, surface ozone concentrations are very variable and composed of very dense and isolated plumes. This explains the large variability of scores when comparing point by point model and surface measurements, even if the horizontal resolution is coarse.

The scores are better for continental stations as Champforgeuil and Agen. The model is able to capture the day-to-day variability, with highest values recorded for 16 and 17 June and 6–10 July. This corresponds to well-established polluted periods, but the maximum values of 140 µg m^{-3} are far from high-pollution events.

6.3 Ozone and meteorological vertical profiles during the ATR flights

The ozone concentrations measured during the ATR flights are averaged from 1 Hz to a 5 mn time step. The number of averaged data is reported in Table 2. The simulated concentrations corresponding to the location of the measurement are interpolated in time (between the two modeled hourly outputs), vertically (between the two model vertical levels) and horizontally (using a bilinear interpolation). The comparison between the modeled and measured ozone concentrations is presented in Fig. 12. The corresponding altitude, temperature (in °C) and mean wind speed (in m s^{-1}) are also presented, using the same abscissa axis.

Each flight lasts between 2 and 3 h. In the altitude panels, we can see that the aircraft made several iso-altitude measurements, mainly at 4000 and 6000 m. For meteorological data, the temperature is always very well simulated by the WRF model. The differences between model and measurements are very weak except, for example, for flights 30 and 31 where the temperature is slightly more underestimated by the model in altitude than close to the surface. The wind is variable and there are differences between simulated values and measurements, mostly in terms of variability, but the absolute values are correctly estimated.

Ozone is always overestimated by the model, especially in altitude. This is probably a direct effect of boundary conditions that may be too strong for this period. The boundary chemical fields are derived from a global climate model and the summer of 2013 was moderated in terms of pollution: the climatology may thus induce a positive bias in the model. These flights within the marine boundary layer are a very good opportunity to evaluate ozone concentrations over the maritime surfaces. These concentrations are usually very high in models due to a lack of deposition. This ozone deposition underestimation is rarely documented and quantified, but some previous studies showed that the dry deposition velocities used over oceans for gaseous species may be underestimated, due to a misrepresented turbulence as pointed out by Garland et al. (1980), Ganzeveld et al. (2009) and Coleman et al. (2010), for example. The differences between the model and observations are lower when the aircraft is under 1000 m a.g.l. (above ground level). Below this altitude, observed ozone concentrations values of up to 60 ppb are not always well captured by the model. This is a direct effect of

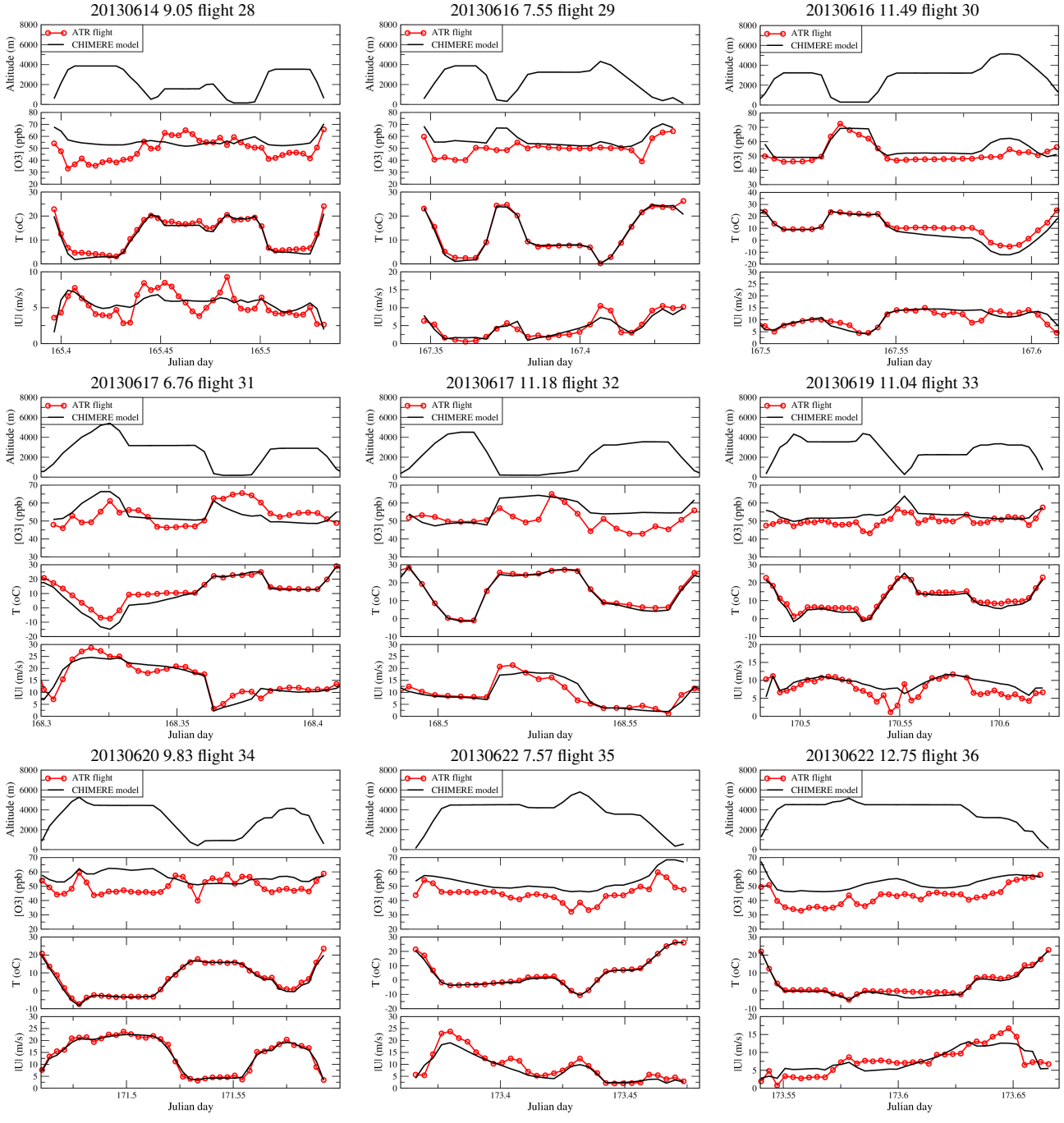

Figure 12. Comparisons between observed and modeled O_3 concentrations, temperature and wind speed along the flight trajectories. The top plot indicates the altitude above sea level of the flight. The abscissa represents the day of the year.

the limitation due to the horizontal resolution, the model being not able to represent local ozone plumes as presented in Fig. 9.

7 Analysis of aerosol optical depth

The AOD quantifies the extinction of radiation by aerosols along the whole atmospheric column. The comparison between model and measurements is widely used to estimate the models' ability to reproduce aerosol plumes. However, comparisons of AOD have limitations. Being vertically integrated, there is no information on the vertical structure of the aerosol plume. In addition, AOD is estimated for a specific wavelength, not always representative of the complete size distributions of all aerosols. In this study, the CHIMERE outputs of AOD are calculated at 600 nm, due to the Fast-J algorithm used in the model.

7.1 Comparisons between MODIS and CHIMERE

As a first step, the satellite measurements are here only used to check if the main AOD patterns are well retrieved by the model. The measured AOD at 550 nm is extracted from the MODIS satellite data over the period from 6 June to 15 July 2013. Observations are interpolated on the model grid and comparisons are done for collocated data in space and time, as displayed in Fig. 13. The MODIS map includes the AOD retrieved over ocean and over land, proposed on the NASA Giovanni database. MODIS AOD products have been used for many years to study the amount and origin of aerosols in the Mediterranean troposphere. Barnaba and Gobbi (2004) used these data to split relative contributions of aerosols on AOD. They showed that for the same particle size, its origin (maritime, continental or desert dust) may induce an AOD variability of one order of magnitude. More recently, Levy et al. (2010) evaluated the MODIS AOD product over land, by comparison to AERONET sunphotometer data. They showed that there is a high correlation ($R = 0.9$) between the two AOD products, with a mean bias of ± 0.05.

The AOD data are time averaged over the period from 6 June to 15 July 2013 in order to have the maximum of available information on the map. Figure 13 shows that, on average for all the considered period, CHIMERE reproduces realistically the main features of the AOD over the considered region, with average values above unity for the Sahelian band and the Arabian Peninsula. However, CHIMERE misses high AOD values on the eastern side of the Caspian Sea as well as over the northern part of the Atlantic. For the first area, the underestimation of the AOD by CHIMERE may be related to missing dust emissions, while for the northern Atlantic, the high AOD values in MODIS are related to an average computed from very few data points, possibly during an event of transport of a polluted plume (e.g., biomass burning or mineral dust) from outside of the simulation domain that is not present in the global climatologies used at the boundaries. Over Europe, AOD is also underestimated where anthropogenic sources dominate.

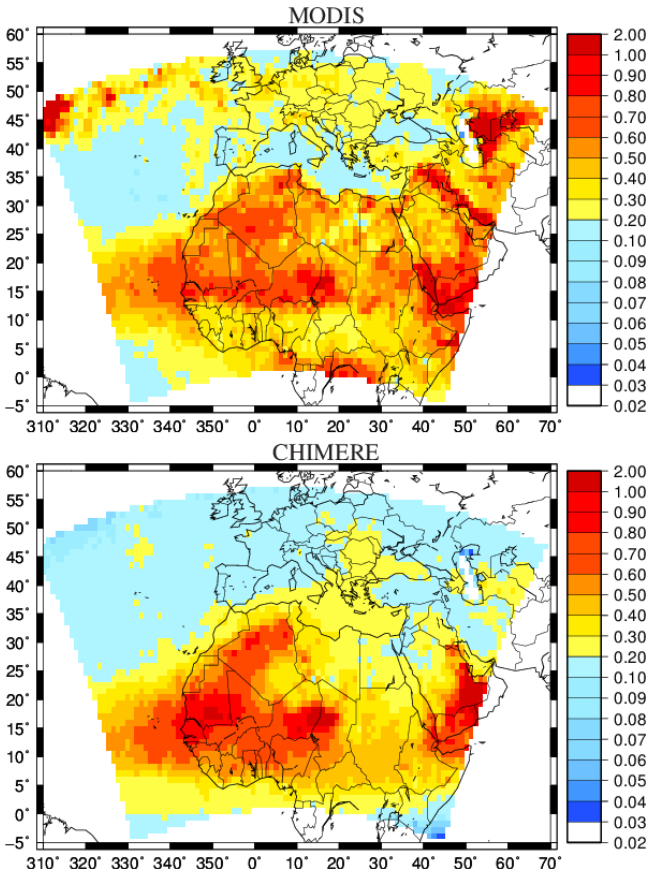

Figure 13. Comparison of AOD measured by MODIS (top) and modeled with CHIMERE (bottom). This AOD corresponds to the mean averaged value over the period from 6 June to 15 July 2013.

7.2 Comparisons between AERONET and CHIMERE

Comparisons between modeled and measured AOD are also done using the AERONET data (level 2; Holben et al., 2001). Time series are presented in Fig. 14. While the station of Banizoumbou is located in a mineral dust source area, the stations of Cabo Verde and Dakar are often influenced by dust outbreaks. This explains that over the whole period, AOD values are high, ranging from 0.4 to 2. The day-to-day variability is also important and these time series show that the highest AOD values are observed during the period from 5 to 15 June. A second period with high values is between 27 and 30 June, with values of up to AOD = 1. The model is able to retrieve the observed day-to-day variability, even if, on average, modeled values are greater than observed ones for stations far away from the main Saharan dust sources.

Time series are also presented for the stations of Lampedusa, Forth Crete and Izana. This set of stations is represen-

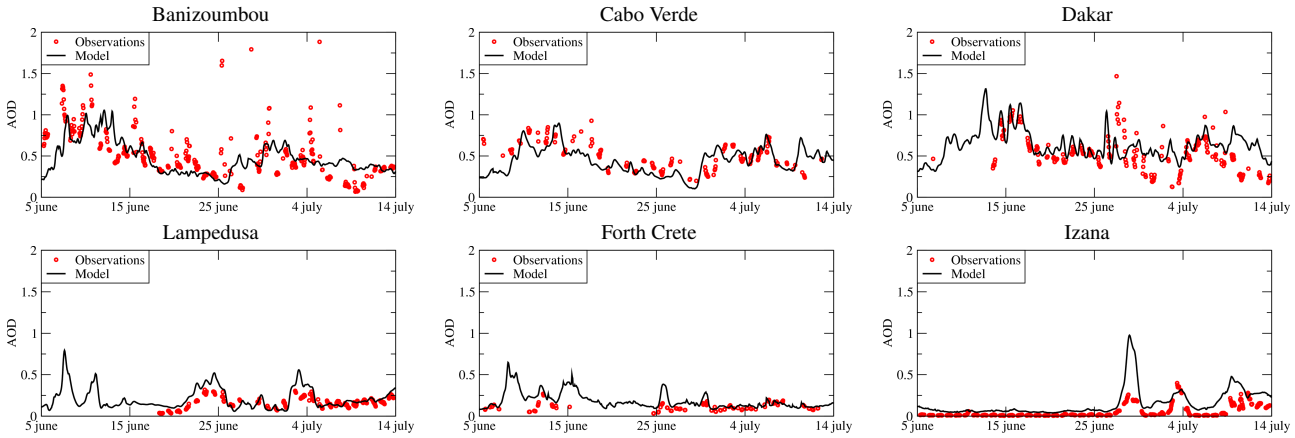

Figure 14. Time series of hourly AOD for selected AERONET stations.

tative of small islands (for Lampedusa and Izana) and remote locations (Forth Crete). The measured AOD values are always lower than 0.5. This clearly shows that, during the whole period, no intense aerosol plume was observed over the Mediterranean Sea. The comparison results are not as good as for the African stations and the model tends to overestimate the AOD over the Mediterranean area. This overestimation may be due to several factors that cannot be diagnosed only with the AOD, this quantity being an integrated budget of many possible contributions. This may be an overestimation of surface mineral dust emissions, a shift in the aerosol size distribution, or an underestimation of modeled dry deposition velocities. However, considering all these potential problems and compared to the AOD of the AERONET measurements, the modeled AOD has not an important bias and follows the observed day-to-day variability. The discrepancies are studied in the last section in terms of the aerosol size distribution.

Table 8 corresponds to statistical scores calculated over these AERONET stations. The number of observations is very variable from one station to another: if the Izana station has 516 measurements, Forth Crete has only 108. These differences are certainly due to the cloud screening algorithm applied on the raw sunphotometer data to ensure that provided AODs are only due to aerosols. The correlation is variable from one site to another with values ranging from 0.20 (Ilorin) to 0.77 (Izana) and 0.79 (Lampedusa). The RMSE is very large, of the order of magnitude of the AOD value, showing important discrepancies between model and measurements. The bias shows that the model underestimates AOD in Africa where are the mineral dust sources and tends, contrarily, to overestimate AOD for sites such as Izana and Lampedusa. This may be due to compensation errors acting differently as a function of the source types and locations: the aerosol size distribution is different between mineral dust and anthropogenic emissions; i.e., the combination of errors in the aerosol size distribution and the emitted flux may provide a correct AOD or not.

Table 8. R, RMSE and bias of measured and modeled hourly AOD, for AERONET stations.

Site	N_{obs}	$\overline{AOD}$ hourly		R	RMSE	Bias
		Obs.	Mod.			
Banizoumbou	357	0.59	0.46	0.27	0.49	−0.12
Cabo Verde	166	0.49	0.46	0.50	0.16	−0.03
Dakar	248	0.53	0.65	0.55	0.23	0.13
Cinzana	338	0.58	0.45	0.58	0.34	−0.13
Ilorin	104	0.38	0.42	0.20	0.35	0.04
Izana	516	0.05	0.15	0.77	0.15	0.10
Lampedusa	238	0.16	0.22	0.79	0.09	0.06
Saada	410	0.24	0.24	0.65	0.15	0.00
Zinder Airport	345	0.56	0.69	0.41	0.43	0.13
Forth Crete	108	0.11	0.17	0.49	0.08	0.06

8 Analysis of PM_{10} surface concentrations

The analysis of PM_{10} surface concentrations is complementary to the analysis of AOD. Comparisons are here presented between surface AirBase measurements and, for the corresponding location in the model domain, PM_{10} concentrations at the model's first vertical level.

8.1 Statistical comparisons between model and observations

Table 9 presents scores for this comparison. The values are daily averaged and are expressed in micrograms per cubic meter. The number of values compared is very variable and mostly between 700 and 1000, corresponding to hourly data over the whole period. Italian stations are different and measurements are only daily, leading to a lower number of raw

Table 9. R, bias and RMSE for the daily mean averaged PM_{10} ($\mu g\,m^{-3}$) surface concentrations (except for the Lampedusa measurements corresponding to total suspended particles).

Site	N_{obs}	PM_{10} daily mean		R	RMSE	Bias
		Obs.	Mod.			
AirBase coastal "background" stations						
Zorita	37	16.1	15.5	0.59	8.9	−0.5
Cartagena	41	21.6	23.1	−0.02	12.7	1.5
Malaga	40	32.5	30.1	−0.09	20.0	−2.4
Ajaccio	33	21.0	27.6	0.15	11.2	6.6
Bastia	40	21.1	25.0	0.09	9.5	3.9
Hyères	41	29.2	25.9	0.68	6.3	−3.3
Taranto	39	19.8	21.4	0.48	7.0	1.6
Chitignano	40	10.4	20.3	0.66	10.8	10.0
AirBase continental "background" stations						
Aranjuez	38	23.1	14.3	0.41	12.8	−8.8
Logroño	41	23.2	14.7	0.46	10.1	−8.5
Cordoba	41	21.2	23.4	0.23	18.1	2.2
Agen	41	14.5	16.6	−0.04	9.7	2.1
Champforgeuil	41	15.8	17.5	0.17	9.7	1.6
Gap	35	13.0	13.5	0.56	4.9	0.5
Baceno	33	7.9	12.6	0.38	8.7	4.8
Schivenoglia	39	27.5	20.6	0.32	12.1	−6.8
Vercelli	36	16.3	19.2	0.68	7.2	2.9

observations. At the end, 33–41 daily averaged values are available. The observed values ranged from 7.9 (Baceno) to 32.5 $\mu g\,m^{-3}$ (Malaga). For the model, the values ranged from 12.6 (Baceno) to 30.1 $\mu g\,m^{-3}$ (Malaga). If the variability from site to site is correctly reproduced, the results showed that the model may underestimate or overestimate the concentrations, depending on the site. There is no obvious link between the location of the site and the sign of the difference: the bias may be positive or negative for sites in the same region. Depending on the station, the correlation ranges from very low (−0.02 for Cartagena and −0.04 for Agen, for example) to moderate (0.66 in Chitignano, 0.68 in Hyères, 0.68 in Vercelli). For 11 stations (on a total of 17), the bias remains lower than $\pm 4\,\mu g\,m^{-3}$.

8.2 Surface concentration time series

The measured and modeled daily averaged surface PM_{10} concentrations are presented in Fig. 15 as time series. On average, the background concentrations are well simulated for all sites. However, some discrepancies appear when some peaks are modeled but not measured, as for example at Zorita, Malaga and Agen. The lower bias on the AOD suggests that the whole column is correct but that the surface concentrations are too large. This can be, partially, a problem of exaggerated vertical diffusion, often diagnosed in deterministic Eulerian models (Vuolo et al., 2009). Another possibility is to have too important local emissions. A way to better understand this overestimation is to analyze the aerosol composition, as presented in the next section.

9 The modeled aerosol speciation

In the previous sections, the aerosol's behavior was analyzed in terms of AOD and surface PM_{10}. In this section, aerosol composition is analyzed and results are presented in terms of time series of surface concentrations and vertical profiles of concentrations.

9.1 Time series

For each site, the modeled aerosol composition is presented as surface time series in Fig. 16. The concentrations are shown for the whole aerosol size distribution, i.e., for a mean mass median diameter D_p from 0.04 to 40 µm. It is thus logical to have surface concentrations higher than the ones presented for the PM_{10} time series. For all time series, the most important contribution comes from mineral dust, with at least 50 % of the total mass. This mineral dust part is also responsible of the large peaks observed in the PM_{10} concentrations. The second most important contribution corresponds to sea salts, specifically for locations corresponding to islands or for coastal sites such as Lampedusa and Cape Corsica. For "continental background" stations such as Champforgeuil and Agen, the concentrations are lower than for other stations and the relative part of sea salt becomes logically negligible. For days when there is no peak of dust and sea salt, sulfate concentrations dominate the aerosol composition. The last most important contribution is from sulfates with large concentrations modeled in Lampedusa and Malaga, among others. Finally, the relative contributions of POM and EC are very low in the total, showing in particular that this period was not influenced by large vegetation fire events.

9.2 Relative contribution of chemical species

The time series presented in the previous section showed the large temporal variability of the surface concentrations as well as the large variability of the aerosol chemical composition. In order to quantify these relative contributions site by site, the relative amount of each chemical species is estimated as a percentage of the total concentration. The calculation is done by cumulating the hourly concentrations over the whole studied period and species per species. The results are presented in Table 10. For each site, the value of the most abundant species is written in bold.

For 13 stations (out of a total of 17 stations), the most important species is mineral dust, with values ranging from 25.01 (Champforgeuil) to 64.48 % (Cordoba). In general, the sites where mineral dust dominates correspond to the western part of the Mediterranean: Zorita, Cartagena, Malaga, Aranjuez, and Cordoba (all these sites being in Spain).

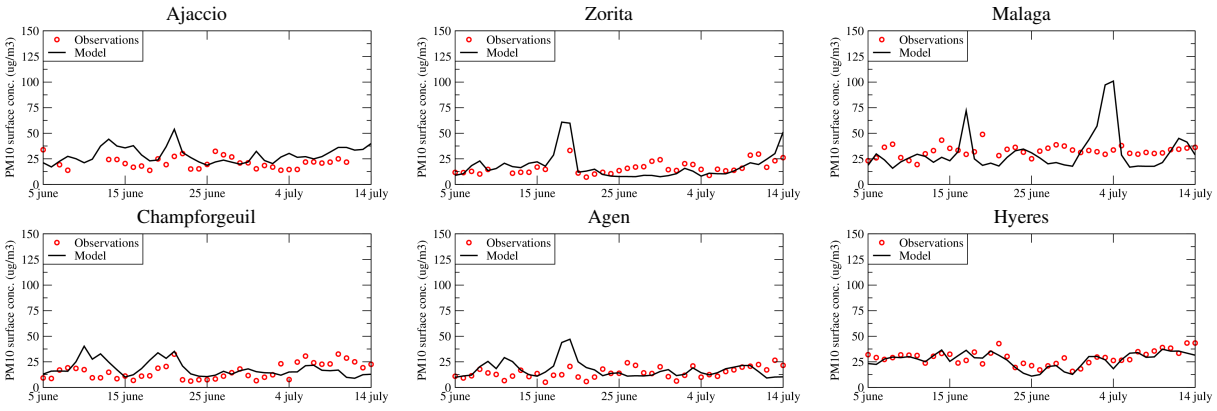

Figure 15. Time series of daily averaged PM_{10} surface concentrations for some selected AirBase sites, continental and coastal stations.

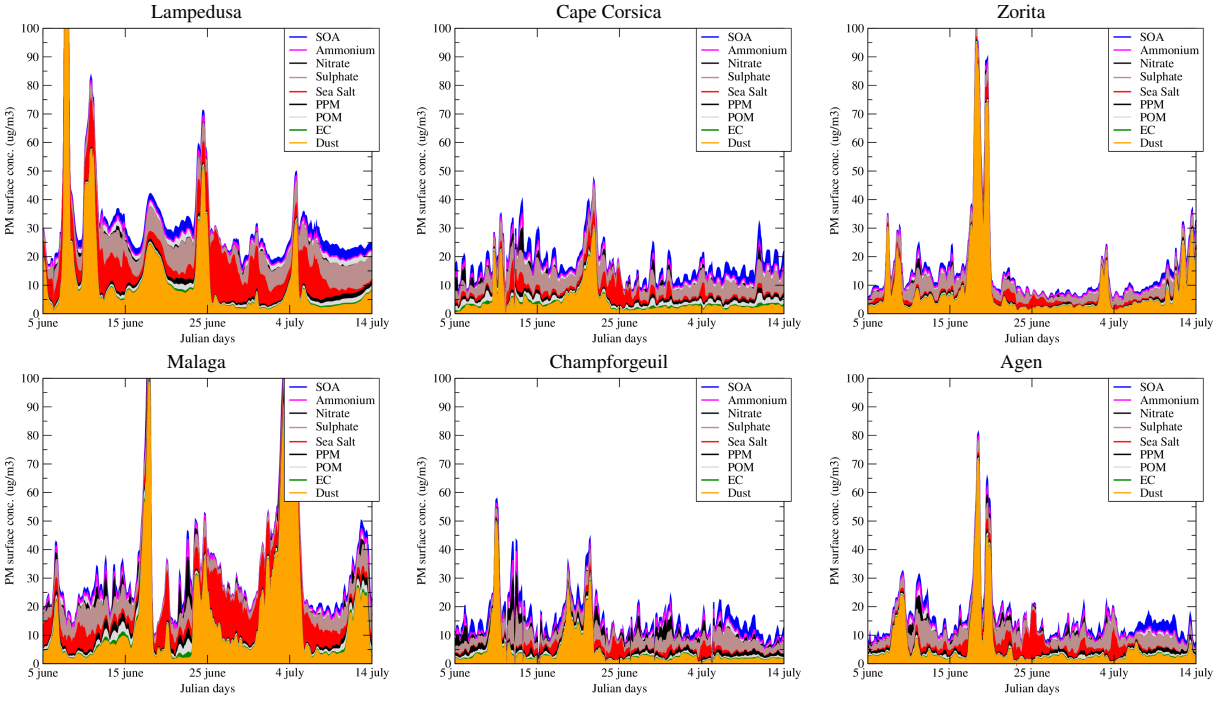

Figure 16. Time series of hourly surface concentrations of PM_{40} constituted by all modeled aerosols for the ADRIMED sites (Lampedusa and Cape Corsica) and some selected AirBase sites, continental and coastal stations.

The second most important contribution is sulfate: this is the most important component for the aerosols at sites Cape Corsica (28.39 %), Ajaccio (22.79 %), Bastia (28.05 %) and Schivenoglia (24.73 %). The first three sites are in Corsica and the last one in the north of Italy. For the sites in Corsica, these large amounts of sulfates are due to shipping emissions or the vicinity of the Fos-Berre industrial area in the south of France, where Schivenoglia is close to industries.

The third most important contribution is sea salt. For sites such as Lampedusa, Cartagena, and Malaga this contribution is close to the sulfate contribution values. All these sites correspond to island or coastal sites and are thus more exposed to sea salt emissions. For all continental sites, the sea salt contribution is low, between 2 (Baceno) and 12.76 % (Agen). Finally, only one site has a major contribution very different from the others: in Hyéres, the most important chemical species is POM (particulate organic matter) and this is most likely due to the proximity of the Fos-Berre area, with organic carbon emissions.

9.3 Vertical profiles

In order to link the information of surface concentrations, aerosol composition and vertical structure, Fig. 17 presents vertical profiles for the same stations as in Fig. 16 and for

Table 10. Relative percentages of the chemical composition of the modeled surface PM_{10} for each site. Values are calculated using the hourly values for the period from 1 June to 15 July 2013. For each site, the largest value is written in bold.

Site	SOA	Ammonium	Nitrate	Sulfate	Sea salt	PPM	POM	EC	Dust
AirBase coastal "background" stations									
Lampedusa	6.17	6.60	0.70	20.20	23.71	2.95	2.86	1.06	**35.75**
Cape Corsica	12.26	10.51	2.57	**28.39**	10.77	5.18	6.95	2.70	20.66
Zorita	5.12	7.20	0.79	19.43	5.95	2.70	2.16	0.74	**55.90**
Cartagena	3.76	6.92	0.71	19.16	19.28	2.74	3.27	1.25	**42.92**
Malaga	3.20	6.12	2.74	14.97	19.35	3.62	4.17	1.64	**44.20**
Ajaccio	13.91	9.40	5.92	**22.79**	11.94	5.96	12.36	4.85	12.88
Bastia	14.36	10.74	2.64	**28.05**	7.84	5.48	7.71	2.99	20.20
Hyères	7.05	6.69	2.65	18.54	12.56	10.56	**23.79**	9.57	8.59
Taranto	9.25	9.21	0.45	25.75	14.21	7.38	4.27	1.69	**27.79**
Chitignano	15.87	10.54	3.67	**26.16**	4.78	7.51	6.50	2.59	22.39
AirBase continental "background" stations									
Aranjuez	3.80	6.69	0.83	17.52	5.50	4.07	3.43	0.93	**57.23**
Logroño	10.03	10.82	4.22	28.25	6.76	3.19	2.34	0.80	**33.60**
Cordoba	2.73	5.39	0.40	14.34	7.29	2.50	2.18	0.68	**64.48**
Agen	9.36	9.67	3.47	24.56	12.76	5.06	3.39	1.35	**30.39**
Champforgeuil	11.46	11.13	8.17	24.93	7.25	6.58	3.79	1.69	**25.01**
Gap	12.68	10.27	4.17	25.63	3.85	6.35	4.07	1.75	**31.24**
Baceno	12.82	10.81	9.39	23.35	2.00	4.89	3.51	1.43	**31.81**
Schivenoglia	14.03	11.04	7.89	**24.73**	3.77	7.93	6.32	2.66	21.63
Vercelli	13.58	9.64	3.17	24.40	2.68	9.08	6.85	2.93	**27.65**

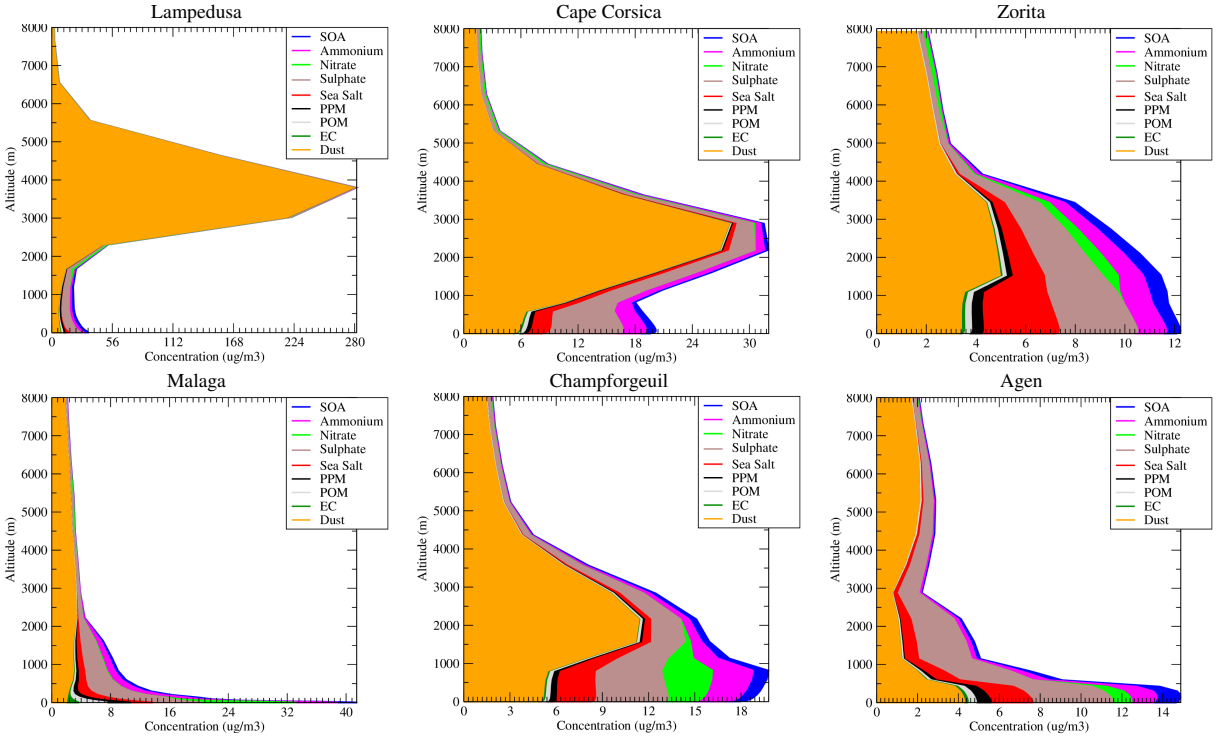

Figure 17. Vertical profiles of all modeled aerosols for 21 June 2013. Results are presented for the ADRIMED sites (Lampedusa and Cape Corsica) and some selected AirBase sites, continental and coastal stations. Note that the abscissa is different in each plot to better see the values.

21 June 2013 at 12:00 UTC. Abscissa scales in the figure are different in order to clearly see all profiles. The largest concentrations are modeled in Lampedusa, with a maximum of 280 µg m^{-3} at 4000 m a.g.l. This maximum is due to the long-range transport: huge concentrations are emitted at the surface in Africa and quickly transported in altitude due to important mixing. These concentrations are injected above the Atlantic Ocean in thin layers and transported towards Mediterranean Sea. A peak of mineral dust in altitude is also modeled in Cape Corsica and Champforgeuil. In Cape Corsica, the maximum value is 30 µg m^{-3} at 2500 m a.g.l., with a contribution of 16 µg m^{-3} from mineral dust.

In Champforgeuil, the most important concentrations are modeled at 1000 m a.g.l., around 19 µg m^{-3}. This peak is constituted of a mixing of sea salt, sulfates, nitrate, ammonium and mineral dust. A secondary peak is observed at 2000 m a.g.l., mainly due to mineral dust and explaining the large vertical extension of the aerosol concentrations.

For Zorita, Malaga and Agen, the maximum concentrations are located close to the surface. They are lower than when mineral dust plumes are modeled, with a maximum from 12 to 40 µg m^{-3}. The aerosol speciation varies for each site, as described in Table 10. Finally, for all these profiles, the mineral dust contribution corresponds to the main part of the aerosol composition in altitude, with important contributions of sulfates, from the surface up to 4000 m.

10 Aerosol size distributions

The way the aerosols can evolve in the atmosphere also depends on their size distribution. Depending on the types of aerosols, abundance will vary according to different size classes. This will cause a different deposition and therefore a different long-range transport. To accurately model the size distribution of aerosols is thus important to track the aerosols over long periods (several days) and large areas (several thousands of kilometers). Unfortunately, the size distribution is difficult to measure and model. In this section, we compare measured and modeled aerosol size distribution in order to see if discrepancies between the model and measurements may be due to a bad representation of this quantity.

10.1 Observed and modeled aerosol size distributions

Observations from the AERONET inversion algorithm results (Dubovik and King, 2000) are used. For each AERONET station, the inversion algorithm provides volume particle size distribution for 15 bins, logarithmically distributed for radii between 0.05 and 15 µm. In CHIMERE, the aerosol size distribution is defined during the emission flux calculations and is different for each species (following the recommendation of the emission inventories, as described in Menut et al., 2013a). For all aerosols (except mineral dust), the distribution is fixed at the emission and then may only vary with heterogeneous chemistry and deposition. For mineral dust, the size distribution may vary at emission, depending on the wind speed and following the dust production model of Alfaro and Gomes (2001). In order to directly compare observations and model results, the modeled column aerosol volume–size distribution is calculated for each model bin as in Péré et al. (2010):

$$\frac{\mathrm{dV}}{d\log(D_p)} = \sum_{k=1}^{k} = \mathrm{nlevels} \frac{\left(\sum_{c=1}^{c=\mathrm{naero}} \frac{m_\mathrm{c}}{\rho_\mathrm{c}} \right) \times \Delta z_\mathrm{k}}{\log(D_{\mathrm{p,\,max}}) - log(D_{\mathrm{p,\,min}})}, \quad (2)$$

where m_c is the mass concentration (the mass of particles in a volume of air, in µg m^{-3}) for the naero modeled aerosols. ρ_c is the particle density (also in µg m^{-3}, the mass of the particle in its own volume). In this model version, all aerosols have the same density, $\rho = 1.5 \times 10^3$ kg m^{-3}, except the mineral dust with $\rho = 2.65 \times 10^3$ kg m^{-3}. Δz_k the model layer thickness (for a total of nlevels levels) and $D_{\mathrm{p,\,min}}$ and $D_{\mathrm{p,\,max}}$ the minimum and maximum mean mass median diameter of the ith bin. These diameters are converted to radii for the direct comparison with the AERONET data. The naero model species are those presented in the previous sections: SOA, ammonium, nitrate, sulfate, sea salt, PPM, POM, EC and dust.

10.2 Results

Retrieved aerosol size distributions are presented in Fig. 18 for some stations listed in Table 1: Banizoumbou, Cinzana, Cabo Verde, Izana and Lampedusa. The aerosol sizes are expressed in radius, as the original AERONET ASD data. In the figures, the scale for the volume size distribution changes for each date and site, in order to clearly see the values.

Maximum concentrations are observed and modeled in Banizoumbou and Cinzana, these stations being where the mineral dust sources are. This also explains that the size distribution is mainly constituted by a mode with r= 1–2 µm, corresponding to a dominant mode in mineral dust emissions, (Alfaro and Gomes, 2001). For these two sites, a systematic difference is observed between the model and the measurements: the main peak of the modeled coarse mode is for a radius of $\approx$ 1 µm, when the AERONET ASD exhibits a peak for a radius of $\approx$ 2 µm. This bias will probably induce a longer transport in the model than in reality, since the deposition velocity increases with the aerosol radius for these particles sizes (Forêt et al., 2006). These results clearly show that improvements have to be done in the size distribution of mineral dust emissions. Even if only a few figures are presented, all size distributions were analyzed and these discrepancies were observed in all cases, highlighting a systematic problem in the model representation.

After some transport of mineral dust, an important fine mode (with $r \approx 0.03$ µm) is modeled at Cabo Verde. This

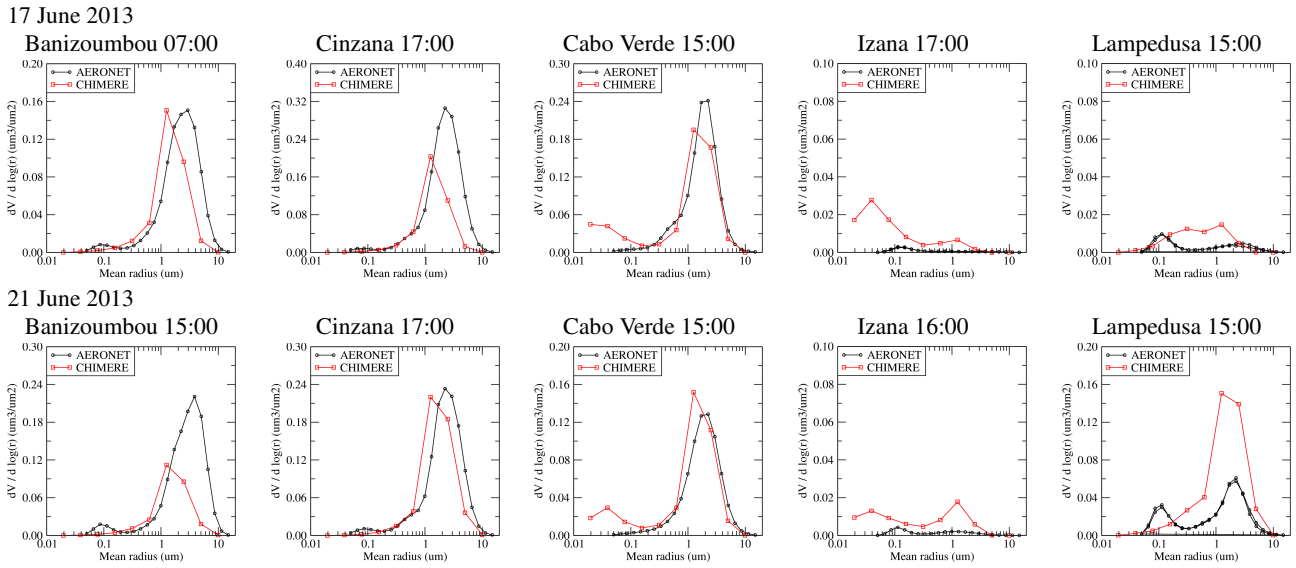

Figure 18. Comparisons between the measured (AERONET) and modeled (CHIMERE) aerosol size distributions for the locations of Banizoumbou, Cinzana, Cabo Verde, Izana and Lampedusa. Distributions are presented for 17 and 21 June 2013, and for hours where the AERONET hourly inverted distributions are available.

fine fraction is not present in the AERONET size distribution. Far from the mineral dust sources, in Izana and Lampedusa, the comparisons of observed and modeled size distributions are poor. In Izana, the model overestimates the AERONET concentrations for all modes. In Lampedusa, observations clearly show two modes (with radius ≈ 0.1 and 2 µm), when the model reproduces a flat distribution for 17 June and a coarse mode peak only for 21 June.

11 Conclusions

This study analyzed the ozone and aerosol tropospheric concentrations and their variability over the Euro–Mediterranean region, from 1 June to 15 July 2013. This region and period was studied within the framework of the ADRIMED project, a measurements campaign of the CHARMEX program. This analysis was performed by using measurements from the ADRIMED project (airborne measurements), routine network measurements (AIRBASE, AERONET, E-OBS) and modeling with WRF and CHIMERE. First, the model results were compared to measurements to quantify the ability of the model to restitute the spatiotemporal variability of ozone and aerosol both at the surface and in altitude. Second, the model was used to go further by analyzing the chemical composition of the aerosols. In addition, the aerosol size distribution variability between Africa and the Mediterranean area was analyzed by comparing AERONET and CHIMERE values.

It was shown that the summer 2013 was not highly polluted compared with the other years. The meteorology, namely 2 m temperature and daily precipitation amount, was characterized using E-OBS data and WRF model results. The meteorological conditions were far from drought and several precipitation events were observed and modeled. This explains a moderate ozone production (sensitive to temperature) and mean values of aerosol concentrations (sensitive to scavenging). In addition to the real situation, the model was found to underestimate the temperature (a bias of $\approx$ 0-1.5 K over land where E-OBS data are available), contributing to slow the already low ozone production. On the other hand, the correct modeled precipitation variability helps to correctly quantify the aerosol variability, with scavenging at the right place and day.

The ozone concentrations were studied along the flight trajectories and close to the surface. If the main day-to-day variability was simulated, it was shown that the model has difficulties to reproduce the numerous ozone plumes, relatively thin but not very concentrated, flowing from west to east in Europe. When precipitation events occurred, the ozone and PM surface concentrations decreased, showing the high impact of photolysis attenuation due to cloudiness for ozone and wet scavenging for aerosols. Using the model aerosol speciation, it was shown that the main part of the PM_{10} surface concentration is composed of mineral dust. Another large fraction is due to sea salt and sulfate concentrations. On the vertical, the mineral dust clearly dominates the total load of aerosols, when sea salt and sulfates are mainly present in the boundary layer. A focus was done on aerosol size distribution by using time series of AERONET products over numerous sites, in Africa, where the sources of mineral dust are and, in Europe, where a mix of several sources is present: local erosion, anthropogenic and biogenic emissions, vegetation fires. The ability of the model to reproduce

the aerosol size distribution was quantified and it was shown that, in Africa, the coarse mode is underestimated when, in the Euro–Mediterranean area, the fine mode is mainly overestimated by the model.

Acknowledgements. This study was partly funded by the French Ministry in charge of Ecology. We thank the SAFIRE joint laboratory and the CHARMEX program for providing us all campaign measurements used in this study. We thank the EEA for maintaining and providing the AirBase database of pollutant surface concentrations over Europe. We thank the principal investigators and their staff for establishing and maintaining the AERONET sites used in this study: Didier Tanré for Banizoumbou, Cabo Verde and Dakar; Bernadette Chatenet and Jean-Louis Rajot for Zinder and Cinzana; Daniela Meloni and Alcide Di Sarra for Lampedusa. We acknowledge the Service d'Observation PHOTONS/AERONET and the AERONET-ACTRIS TNA supporting the AERONET activity in Europe. Analyses and visualizations used in this study for the MODIS satellite AOD maps were produced with the Giovanni online data system, developed and maintained by the NASA GES DISC. We acknowledge the E-OBS data set from the EU-FP6 project ENSEMBLES (http://ensembles-eu.metoffice.com) and the data providers in the ECAD project (http://www.ecad.eu).

Edited by: O. Dubovik

References

Alfaro, S. C. and Gomes, L.: Modeling mineral aerosol production by wind erosion: Emission intensities and aerosol size distribution in source areas, J. Geophys. Res., 106, 18075–18084, 2001.

Barnaba, F. and Gobbi, G. P.: Aerosol seasonal variability over the Mediterranean region and relative impact of maritime, continental and Saharan dust particles over the basin from MODIS data in the year 2001, Atmos. Chem. Phys., 4, 2367–2391, doi:10.5194/acp-4-2367-2004, 2004.

Basart, S., Pérez, C., Cuevas, E., Baldasano, J. M., and Gobbi, G. P.: Aerosol characterization in Northern Africa, Northeastern Atlantic, Mediterranean Basin and Middle East from direct-sun AERONET observations, Atmos. Chem. Phys., 9, 8265–8282, doi:10.5194/acp-9-8265-2009, 2009.

Bergamo, A., Tafuro, A. M., Kinne, S., De Tomasi, F., and Perrone, M. R.: Monthly-averaged anthropogenic aerosol direct radiative forcing over the Mediterranean based on AERONET aerosol properties, Atmos. Chem. Phys., 8, 6995–7014, doi:10.5194/acp-8-6995-2008, 2008.

Bessagnet, B., Hodzic, A., Vautard, R., Beekmann, M., Cheinet, S., Honoré, C., Liousse, C., and Rouil, L.: Aerosol modeling with CHIMERE: preliminary evaluation at the continental scale, Atmos. Environ., 38, 2803–2817, 2004.

Bian, H., , and Prather, M.: Fast-J2: accurate simulation of stratospheric photolysis in global chemical models, J Atmos Chem, 41, 281–296, 2002.

Briant, R., Menut, L., Siour, G., and Prigent, C.: Homogeneized modeling of mineral dust emissions over Europe and Africa using the CHIMERE model, Geosci. Model Dev. Discuss., 7, 3441–3480, doi:10.5194/gmdd-7-3441-2014, 2014.

Chen, F. and Dudhia, J.: Coupling an advanced land surface-hydrology model with the Penn State-NCAR MM5 modeling system. Part I: Model implementation and sensitivity, Mon. Weather Rev., 129, 569–585, 2001.

Coleman, L., Varghese, S., Tripathi, O., Jennings, S., and O'Dowd, C.: Regional-Scale Ozone Deposition to North-East Atlantic Waters, Advances in Meteorology, 2010, 243–701, doi:10.1155/2010/243701, 2010.

Colette, A., Ancellet, G., Menut, L., and Arnold, S. R.: A Lagrangian analysis of the impact of transport and transformation on the ozone stratification observed in the free troposphere during the ESCOMPTE campaign, Atmos. Chem. Phys., 6, 3487–3503, doi:10.5194/acp-6-3487-2006, 2006.

Cros, B., Durand, P., Cachier, H., Drobinski, P., Fréjafon, E., Kottmeir, C., Perros, P., Peuch, V.-H., Ponche, J.-L., Robin, D., Said, F., Toupance, G., and Wortham, H.: The ESCOMPTE program: an overview, Atmos. Res., 69, 241–279, 2004.

de la Paz, D., Vedrenne, M., Borge, R., Lumbreras, J., de Andrés, J. M., Pérez, J., Rodriguez, E., Karanasiou, A., Moreno, T., Boldo, E., and Linares, C.: Modelling Saharan dust transport into the Mediterranean basin with CMAQ, Atmos. Environ., 70, 337–350, doi:10.1016/j.atmosenv.2013.01.013, 2013.

di Sarra, A., Pace, G., Meloni, D., De Silvestri, L., Piacentino, S., and Monteleone, F.: Surface shortwave radiative forcing of different aerosol types in the central Mediterranean, Geophys. Res. Lett., 35, L02714, doi:10.1029/2007GL032395, 2008.

Dubovik, O. and King, M. D.: A flexible inversion algorithm for retrieval of aerosol optical properties from Sun and sky radiance measurements, J. Geophys. Res.-Atmos., 105, 20673–20696, doi:10.1029/2000JD900282, 2000.

Dulac, F. and Chazette, P.: Airborne study of a multi-layer aerosol structure in the eastern Mediterranean observed with the airborne polarized lidar ALEX during a STAAARTE campaign (7 June 1997), Atmos. Chem. Phys., 3, 1817–1831, doi:10.5194/acp-3-1817-2003, 2003.

Dulac, F., Arboledas, L. A., Alastuey, A., Ancellet, G., Arndt, J., Attié, J.-L., Augustin, P., Becagli, S., Bergametti, G., Bocquet, M., Bordier, F., Bourdon, A., Bourrianne, T., Bravo-Aranda, J., Carrer, D., Ceamanos, X., Chazette, P., Chiapello, I., Comeron, A., D'Amico, G., D'Anna, B., Delbarre, H., Denjean, C., Desboeufs, K., Descloitres, J., Diouri, M., Biagio, C. D., Iorio, T. D., Sarra, G. D., Doppler, L., Durand, P., Amraoui, L. E., Ellul, R., Ferré, H., Fleury, L., Formenti, P., Freney, E., Gaimoz, C., Gerasopoulos, E., Goloub, P., Gomez-Amo, J., Granados-Munoz, M., Grand, N., Grobner, J., Rascado, J.-L. G., Guieu, C., Hadjimitsis, D., Hamonou, E., Hansson, H., Iarlori, M., Ioannou, S., Jambert, C., Jaumouillé, E., Jeannot, M., Junkermann, W., Keleshis, C., Kokkalis, P., Lambert, D., Laurent, B., Léon, J.-F., Liousse, C., Bartolome, M. L., Losno, R., Mallet, M., Mamouri, R.-E., Meloni, D., Menut, L., Montoux, N., Baquero, R. M., Nabat, P., Navas-Guzman, F., Nicolae, D., Nicolas, J., Notton, G., Ohayon, W., Paoli, C., Papayannis, A., Pelon, J., Pey, J., Pont, V., Pujadas, M., Querol, X., Ravetta, F., Renard, J.-B., Rizi, V., Roberts, G., Roujean, J.-L., Sartelet, K., Savelli, J.-L., Sciare, J., Sellegri, K., Sferlazzo, D., Sicard, M., Smyth, A., Solmon, F., Tanré, D., Torres, B., Totems, J., Sanchez, A. T., Verdier, N., Vignelles, D., Vincent, J., Wagner, F., Wang, Y., Wenger, J., and Yassaa, N.: Overview of the Project ChArMEx activities on Saharan Dust in the Mediterranean region, in: 7th Int. Workshop on

Sand/Duststorms and Associated Dustfall, 2–4 Dec. 2013, Frascati, Italy, 2013.

Forêt, G., Bergametti, G., Dulac, F., and Menut, L.: An optimized particle size bin scheme for modeling mineral dust aerosol, J. Geophys. Res., 111, D17310, doi:10.1029/2005JD006797, 2006.

Ganzeveld, L., Helmig, D., Fairall, C. W., Hare, J., and Pozzer, A.: Atmosphere-ocean ozone exchange: A global modeling study of biogeochemical, atmospheric, and waterside turbulence dependencies, Global Biogeochem. Cy., 23, 1944–9224, doi:10.1029/2008GB003301, 2009.

Garland, J. A., Elzerman, A. W., and Penkett, S. A.: The mechanism for dry deposition of ozone to seawater surfaces, J. Geophys. Res.-Oceans, 85, 7488–7492, doi:10.1029/JC085iC12p07488, 1980.

Gerasopoulos, E., Kouvarakis, G., Vrekoussis, M., Kanakidou, M., and Mihalopoulos, N.: Ozone variability in the marine boundary layer of the eastern Mediterranean based on 7-year observations, J. Geophys. Res., 110, D15309, doi:10.1029/2005JD005991, 2005.

Ginoux, P., Chin, M., Tegen, I., Prospero, J. M., Holben, B., Dubovik, O., and Lin, S. J.: Sources and distributions of dust aerosols simulated with the GOCART model, J. Geophys. Res., 106, 20255–20273, 2001.

Grell, G. A. and Devenyi, D.: A generalized approach to parameterizing convection combining ensemble and data assimilation techniques, Geophys. Res. Lett., 29, 1693, 2002.

Guenther, A., Karl, T., Harley, P., Wiedinmyer, C., Palmer, P. I., and Geron, C.: Estimates of global terrestrial isoprene emissions using MEGAN (Model of Emissions of Gases and Aerosols from Nature), Atmos. Chem. Phys., 6, 3181–3210, doi:10.5194/acp-6-3181-2006, 2006.

Guerreiro, C., de Leuw, F., and Foltescu, V.: Air quality in Europe, European Environment Agency, report, 9, 112 pp., 2013.

Haylock, M. R., Hofstra, N., Tank, A. M. G. K., Klok, E. J., Jones, P. D., and New, M.: A European daily high-resolution gridded data set of surface temperature and precipitation for 1950-2006, J. Geophys. Res.-Atmos., 113, doi:10.1029/2008JD010201, 2008.

Holben, B., Tanre, D., Smirnov, A., Eck, T. F., Slutsker, I., Abuhassan, N., Newcomb, W. W., Schafer, J., Chatenet, B., Lavenu, F., Kaufman, Y. J., Vande Castle, J., Setzer, A., Markham, B., Clark, D., Frouin, R., Halthore, R., Karnieli, A., O'Neill, N. T., Pietras, C., Pinker, R. T., Voss, K., and Zibordi, G.: An emerging ground-based aerosol climatology: Aerosol Optical Depth from AERONET, J. Geophys. Res., 106, 12067–12097, 2001.

Hong, S. Y., Dudhia, J., and Chen, S.: A revised approach to ice microphysical processes for the bulk parameterization of clouds and precipitation, Mon. Weather Rev., 132, 103–120, 2004.

Hong, S. Y., Noh, Y., and Dudhia, J.: A new vertical diffusion package with an explicit treatment of entrainment processes, Mon Weather. Rev., 134, 2318–2341, doi:10.1175/MWR3199.1, 2006.

Israelevich, P., Ganor, E., Alpert, P., Kishcha, P., and Stupp, A.: Predominant transport paths of Saharan dust over the Mediterranean Sea to Europe, J. Geophys. Res., 117, D02205, doi:10.1029/2011JD016482, 2012.

Jiménez-Guerrero, P., Jorba, O., Pay, M. T., Montávez, J. P., Jerez, S., Gómez-Navarro, J. J., and Baldasano, J. M.: Comparison of two different sea-salt aerosol schemes as implemented in air quality models applied to the Mediterranean Basin, Atmos. Chem. Phys., 11, 4833–4850, doi:10.5194/acp-11-4833-2011, 2011.

Kalabokas, P., Mihalopoulos, N., Ellul, R., Kleanthous, S., and Repapis, C.: An investigation of the meteorological and photochemical factors influencing the background rural and marine surface ozone levels in the Central and Eastern Mediterranean, Atmos. Environ., 42, 7894–7906, doi:10.1016/j.atmosenv.2008.07.009, 2008.

Kalnay, E., Kanamitsu, M., Kistler, R., Collins, W., Deaven, D., Gandin, L., Iredell, M., Saha, S., White, G., Woollen, J., Zhu, Y., Chelliah, M., Ebisuzaki, W., Higgins, W., Janowiak, J., Mo, K., Ropelewski, C., Wang, J., Leetmaa, A., Reynolds, R., Jenne, R., and Joseph, D.: The NCEP/NCAR 40-year reanalysis project, Bull. Amer. Meteorol. Soc., doi:10.1175/1520-0477(1996)077, 437–471, 1996.

Kubilay, N., Cokacar, T., and Oguz, T.: Optical properties of mineral dust outbreaks over the northeastern Mediterranean, J. Geophys. Res., 108, 4666D21, doi:10.1029/2003JD003798D, 2003.

Kuenen, J. J. P., Visschedijk, A. J. H., Jozwicka, M., and Denier van der Gon, H. A. C.: TNO-MACC_II emission inventory; a multi-year (2003–2009) consistent high-resolution European emission inventory for air quality modelling, Atmos. Chem. Phys., 14, 10963–10976, doi:10.5194/acp-14-10963-2014, 2014.

Kulmala, M., Asmi, A., Lappalainen, H. K., Baltensperger, U., Brenguier, J.-L., Facchini, M. C., Hansson, H.-C., Hov, Ø., O'Dowd, C. D., Pöschl, U., Wiedensohler, A., Boers, R., Boucher, O., de Leeuw, G., Denier van der Gon, H. A. C., Feichter, J., Krejci, R., Laj, P., Lihavainen, H., Lohmann, U., McFiggans, G., Mentel, T., Pilinis, C., Riipinen, I., Schulz, M., Stohl, A., Swietlicki, E., Vignati, E., Alves, C., Amann, M., Ammann, M., Arabas, S., Artaxo, P., Baars, H., Beddows, D. C. S., Bergström, R., Beukes, J. P., Bilde, M., Burkhart, J. F., Canonaco, F., Clegg, S. L., Coe, H., Crumeyrolle, S., D'Anna, B., Decesari, S., Gilardoni, S., Fischer, M., Fjaeraa, A. M., Fountoukis, C., George, C., Gomes, L., Halloran, P., Hamburger, T., Harrison, R. M., Herrmann, H., Hoffmann, T., Hoose, C., Hu, M., Hyvärinen, A., Hörrak, U., Iinuma, Y., Iversen, T., Josipovic, M., Kanakidou, M., Kiendler-Scharr, A., Kirkevåg, A., Kiss, G., Klimont, Z., Kolmonen, P., Komppula, M., Kristjánsson, J.-E., Laakso, L., Laaksonen, A., Labonnote, L., Lanz, V. A., Lehtinen, K. E. J., Rizzo, L. V., Makkonen, R., Manninen, H. E., McMeeking, G., Merikanto, J., Minikin, A., Mirme, S., Morgan, W. T., Nemitz, E., O'Donnell, D., Panwar, T. S., Pawlowska, H., Petzold, A., Pienaar, J. J., Pio, C., Plass-Duelmer, C., Prévôt, A. S. H., Pryor, S., Reddington, C. L., Roberts, G., Rosenfeld, D., Schwarz, J., Seland, Ø., Sellegri, K., Shen, X. J., Shiraiwa, M., Siebert, H., Sierau, B., Simpson, D., Sun, J. Y., Topping, D., Tunved, P., Vaattovaara, P., Vakkari, V., Veefkind, J. P., Visschedijk, A., Vuollekoski, H., Vuolo, R., Wehner, B., Wildt, J., Woodward, S., Worsnop, D. R., van Zadelhoff, G.-J., Zardini, A. A., Zhang, K., van Zyl, P. G., Kerminen, V.-M., S Carslaw, K., and Pandis, S. N.: General overview: European Integrated project on Aerosol Cloud Climate and Air Quality interactions (EUCAARI) –integrating aerosol research from nano to global scales, Atmos. Chem. Phys., 11, 13061–13143, doi:10.5194/acp-11-13061-2011, 2011.

Lelieveld, J., Berresheim, H., Borrmann, S., Crutzen, P. J., Dentener, F. J., Fischer, H., Feichter, J., Flatau, P. J., Heland,

J., Holzinger, R., Korrmann, R., Lawrence, M. G., Levin, Z., Markowicz, K. M., Mihalopoulos, N., Minikin, A., Ramanathan, V., Reus, M. d., Roelofs, G. J., Scheeren, H. A., Sciare, J., Schlager, H., Schultz, M., Siegmund, P., Steil, B., Stephanou, E. G., Stier, P., Traub, M., Warneke, C., Williams, J., and Ziereis, H.: Global Air Pollution Crossroads over the Mediterranean, Science, 298, 794–799, 2002.

Levy, R. C., Remer, L. A., Kleidman, R. G., Mattoo, S., Ichoku, C., Kahn, R., and Eck, T. F.: Global evaluation of the Collection 5 MODIS dark-target aerosol products over land, Atmos. Chem. Phys., 10, 10399–10420, doi:10.5194/acp-10-10399-2010, 2010.

Mailler, S., Khvorostyanov, D., and Menut, L.: Impact of the vertical emission profiles on background gas-phase pollution simulated from the EMEP emissions over Europe, Atmos. Chem. Phys., 13, 5987–5998, doi:10.5194/acp-13-5987-2013, 2013.

Mailler, S., Menut, L., di Sarra, A. G., Becagli, S., Di Iorio, T., Formenti, P., Bessagnet, B., Briant, Régis, Luis Gómez-Amo, J., Mallet, M., Rea, Géraldine, Siour, G., Sferlazzo, D. M., Traversi, R., Udisti, R., and Turquety, S.: On the radiative impact of aerosols on photolysis rates: comparison of simulations and observations in the Lampedusa island during the ChArMEx/ADRIMED campaign, Atmos. Chem. Phys. Discuss., 15, 7585–7643, doi:10.5194/acpd-15-7585-2015, 2015.

Mallet, M.: Overview of the Chemistry-Aerosol Mediterranean Experiment/Aerosol Direct Radiative Forcing on the Mediterranean Climate (ChArMEx/ADRIMED) summer 2013 campaign, Atelier de Modèlisation de l'Atmosphère, 20–22 January 2014, Toulouse, France, 2014.

Mallet, M., Dubovik, O., Nabat, P., Dulac, F., Kahn, R., Sciare, J., Paronis, D., and Léon, J. F.: Absorption properties of Mediterranean aerosols obtained from multi-year ground-based remote sensing observations, Atmos. Chem. Phys., 13, 9195–9210, doi:10.5194/acp-13-9195-2013, 2013.

Marécal, V., Peuch, V.-H., Andersson, C., Andersson, S., Arteta, J., Beekmann, M., Benedictow, A., Bergström, R., Bessagnet, B., Cansado, A., Chéroux, F., Colette, A., Coman, A., Curier, R. L., Denier van der Gon, H. A. C., Drouin, A., Elbern, H., Emili, E., Engelen, R. J., Eskes, H. J., Foret, G., Friese, E., Gauss, M., Giannaros, C., Guth, J., Joly, M., Jaumouillé, E., Josse, B., Kadygrov, N., Kaiser, J. W., Krajsek, K., Kuenen, J., Kumar, U., Liora, N., Lopez, E., Malherbe, L., Martinez, I., Melas, D., Meleux, F., Menut, L., Moinat, P., Morales, T., Parmentier, J., Piacentini, A., Plu, M., Poupkou, A., Queguiner, S., Robertson, L., Rouïl, L., Schaap, M., Segers, A., Sofiev, M., Thomas, M., Timmermans, R., Valdebenito, Á., van Velthoven, P., van Versendaal, R., Vira, J., and Ung, A.: A regional air quality forecasting system over Europe: the MACC-II daily ensemble production, Geosci. Model Dev. Discuss., 8, 2739–2806, doi:10.5194/gmdd-8-2739-2015, 2015.

Menut, L., Coll, I., and Cautenet, S.: Impact of meteorological data resolution on the forecasted ozone concentrations during the ESCOMPTE IOP 2a and 2b, Atmos. Res., 74, 139–159, 2005.

Menut, L., Goussebaile, A., Bessagnet, B., Khvorostiyanov, D., and Ung, A.: Impact of realistic hourly emissions profiles on modelled air pollutants concentrations, Atmos. Environ., 49, 233–244, 2012.

Menut, L., Bessagnet, B., Khvorostyanov, D., Beekmann, M., Blond, N., Colette, A., Coll, I., Curci, G., Foret, G., Hodzic, A., Mailler, S., Meleux, F., Monge, J.-L., Pison, I., Siour, G., Turquety, S., Valari, M., Vautard, R., and Vivanco, M. G.: CHIMERE 2013: a model for regional atmospheric composition modelling, Geosci. Model Dev., 6, 981–1028, doi:10.5194/gmd-6-981-2013, 2013a.

Menut, L., Perez Garcia-Pando, C., Haustein, K., Bessagnet, B., Prigent, C., and Alfaro, S.: Relative impact of roughness and soil texture on mineral dust emission fluxes modeling, J. Geophys. Res., 118, 6505–6520, doi:10.1002/jgrd.50313, 2013b.

Menut, L., Tripathi, O., Colette, A., Vautard, R., Flaounas, E., and Bessagnet, B.: Evaluation of regional climate simulations for air quality modelling purposes, Clim. Dyn., 40, 2515–2533, doi:10.1007/s00382-012-1345-9, 2013c.

Middleton, N. J. and Goudie, A. S.: Saharan dust: sources and trajectories, T. I. Brit. Geogr., 26, 165–181, doi:10.1111/1475-5661.00013, 2001.

Millan, M., Estrela, M. J., Sanz, M. J., Mantilla, E., Martan, M., Pastor, F., Salvador, R., Vallejo, R., Alonso, L., Gangoiti, G., Ilardia, J., Navazo, M., Albizuri, A., Artano, B., Ciccioli, P., Kallos, G., Carvalho, R. A., Andreas, D., Hoff, A., Werhahn, J., and Seufert, G., and Versino, B.: Climatic Feedbacks and Desertification: The Mediterranean Model, J. Climate, 18, 684–701, 2005.

Mlawer, E., Taubman, S., Brown, P., Iacono, M., and Clough, S.: Radiative transfer for inhomogeneous atmospheres: RRTM a validated correlated-k model for the longwave, J. Geophys. Res., 102, 16663–16682, 1997.

Monks, P., Granier, C., Fuzzi, S., Stohl, A., Williams, M., Akimoto, H., Amann, M., Baklanov, A., Baltensperger, U., Bey, I., Blake, N., Blake, R., Carslaw, K., Cooper, O., Dentener, F., Fowler, D., Fragkou, E., Frost, G., Generoso, S., Ginoux, P., Grewe, V., Guenther, A., Hansson, H., Henne, S., Hjorth, J., Hofzumahaus, A., Huntrieser, H., Isaksen, I., Jenkin, M., Kaiser, J., Kanakidou, M., Klimont, Z., Kulmala, M., Laj, P., Lawrence, M., Lee, J., Liousse, C., Maione, M., McFiggans, G., Metzger, A., Mieville, A., Moussiopoulos, N., Orlando, J., O'Dowd, C., Palmer, P., Parrish, D., Petzold, A., Platt, U., Pöschl, U., Prévôt, A., Reeves, C., Reimann, S., Rudich, Y., Sellegri, K., Steinbrecher, R., Simpson, D., ten Brink, H., Theloke, J., van der Werf, G., Vautard, R., Vestreng, V., Vlachokostas, C., and von Glasow, R.: Atmospheric composition change – global and regional air quality, Atmos. Environ., 43, 5268–5350, 2009.

Moulin, C., Lambert, C. E., Dayan, U., Masson, V., Ramonet, M., Bousquet, P., Legrand, M., Balkanski, Y. J., Guelle, W., Marticorena, B., Bergametti, G., and Dulac, F.: Satellite climatology of African dust transport in the Mediterranean atmosphere, J. Geophys. Res.-Atmos., 103, 13137–13144, doi:10.1029/98JD00171, 1998.

Nabat, P., Solmon, F., Mallet, M., Kok, J. F., and Somot, S.: Dust emission size distribution impact on aerosol budget and radiative forcing over the Mediterranean region: a regional climate model approach, Atmos. Chem. Phys., 12, 10545–10567, doi:10.5194/acp-12-10545-2012, 2012.

Nabat, P., Somot, S., Mallet, M., Sevault, F., Chiacchio, M., and Wild, M.: Direct and semi-direct aerosol radiative effect on the Mediterranean climate variability using a coupled regional climate system model, Clim. Dyn., 44, 1–29, doi:10.1007/s00382-014-2205-6, 2014.

Papayannis, A., Amiridis, V., Mona, L., Tsaknakis, G., Balis, D., Bösenberg, J., Chaikovski, A., De Tomasi, F., Grigorov, I., Mattis, I., Mitev, V., Müller, D., Nickovic, S., Pérez, C., Pietruczuk,

A., Pisani, G., Ravetta, F., Rizi, V., Sicard, M., Trickl, T., Wiegner, M., Gerding, M., Mamouri, R. E., D'Amico, G., and Pappalardo, G.: Systematic lidar observations of Saharan dust over Europe in the frame of EARLINET (2000–2002), J. Geophys. Res.-Atmos., 113, D10204, doi:10.1029/2007JD009028, 2008.

Pappalardo, G., Amodeo, A., Apituley, A., Comeron, A., Freudenthaler, V., Linné, H., Ansmann, A., Bösenberg, J., D'Amico, G., Mattis, I., Mona, L., Wandinger, U., Amiridis, V., Alados-Arboledas, L., Nicolae, D., and Wiegner, M.: EARLINET: towards an advanced sustainable European aerosol lidar network, Atmos. Meas. Tech., 7, 2389–2409, doi:10.5194/amt-7-2389-2014, 2014.

Péré, J., Mallet, M., Pont, V., and Bessagnet, B.: Evaluation of an aerosol optical scheme in the chemistry-transport model CHIMERE, Atmos. Environ., 44, 3688–3699, 2010.

Pérez, C., Haustein, K., Janjic, Z., Jorba, O., Huneeus, N., Baldasano, J. M., Black, T., Basart, S., Nickovic, S., Miller, R. L., Perlwitz, J. P., Schulz, M., and Thomson, M.: Atmospheric dust modeling from meso to global scales with the online NMMB/BSC-Dust model –Part 1: Model description, annual simulations and evaluation, Atmos. Chem. Phys., 11, 13001–13027, doi:10.5194/acp-11-13001-2011, 2011.

Querol, X., Pey, J., Pandolfi, M., Alastuey, A., Cusack, M., Pereza, N., Moreno, T., Viana, M., Mihalopoulos, N., Kallo, G., and Kleanthous, S.: African dust contributions to mean ambient PM10 mass-levels across the Mediterranean Basin, Atmos. Environ., 43, 4266–4277, 2009.

Richards, N. A. D., Arnold, S. R., Chipperfield, M. P., Miles, G., Rap, A., Siddans, R., Monks, S. A., and Hollaway, M. J.: The Mediterranean summertime ozone maximum: global emission sensitivities and radiative impacts, Atmos. Chem. Phys., 13, 2331–2345, doi:10.5194/acp-13-2331-2013, 2013.

Roelofs, G. J., Scheeren, H. A., Heland, J., Ziereis, H., and Lelieveld, J.: A model study of ozone in the eastern Mediterranean free troposphere during MINOS (August 2001), Atmos. Chem. Phys., 3, 1199–1210, doi:10.5194/acp-3-1199-2003, 2003.

Santese, M., Perrone, M. R., Zakey, A. S., De Tomasi, F., and Giorgi, F.: Modeling of Saharan dust outbreaks over the Mediterranean by RegCM3: case studies, Atmos. Chem. Phys., 10, 133–156, doi:10.5194/acp-10-133-2010, 2010.

Skamarock, W., Klemp, J., Dudhia, J., Gill, D., Barker, D., Wang, W., and Powers, J.: A Description of the Advanced Research WRF Version 2, NCAR Technical Note, Boulder, Colorado, USA, 123 pp., 2007.

Spyrou, C., Kallos, G., Mitsakou, C., Athanasiadis, P., Kalogeri, C., and Iacono, M. J.: Modeling the radiative effects of desert dust on weather and regional climate, Atmos. Chem. Phys., 13, 5489–5504, doi:10.5194/acp-13-5489-2013, 2013.

Szopa, S., Foret, G., Menut, L., and Cozic, A.: Impact of large scale circulation on European summer surface ozone: consequences for modeling, Atmos. Environ., 43, 1189–1195, doi:10.1016/j.atmosenv.2008.10.039, 2009.

Turquety, S., Menut, L., Bessagnet, B., Anav, A., Viovy, N., Maignan, F., and Wooster, M.: APIFLAME v1.0: high-resolution fire emission model and application to the Euro-Mediterranean region, Geosci. Model Dev., 7, 587–612, doi:10.5194/gmd-7-587-2014, 2014.

Vogel, B., Vogel, H., Bäumer, D., Bangert, M., Lundgren, K., Rinke, R., and Stanelle, T.: The comprehensive model system COSMO-ART – Radiative impact of aerosol on the state of the atmosphere on the regional scale, Atmos. Chem. Phys., 9, 8661–8680, doi:10.5194/acp-9-8661-2009, 2009.

Von Storch, H., Langenberg, H., and Feser, F.: A spectral nudging technique for dynamical downscaling purposes, Mon. Wea. Rev., 128, 3664–3673, 2000.

Vuolo, M., Chepfer, H., Menut, L., and Cezana, G.: Comparison of mineral dust layers vertical structures modelled with CHIMERE-DUST and observed with the CALIOP lidar, J. Geophys. Res., 114, D09214, doi:10.1029/2008JD011219, 2009.

Wild, O., Zhu, X., and Prather, M. J.: Fast-J: Accurate Simulation of In- and Below-Cloud Photolysis in Tropospheric Chemical Models, J. Atmos. Chem., 37, 245–282, 2000.